

The Sharpness Disparity Principle in Transformers for Accelerating Language Model Pre-Training

Jinbo Wang^{1,*} Mingze Wang^{1,*} Zhanpeng Zhou^{3,*}
 Junchi Yan³ Weinan E^{1,2,4} Lei Wu^{1,2}

¹School of Mathematical Sciences, Peking University

²Center for Machine Learning Research, Peking University

³Sch. of Computer Science & Sch. of Artificial Intelligence, Shanghai Jiao Tong University

⁴AI for Science Institute, Beijing

{mingzewang, wangjinbo}@stu.pku.edu.cn

{zzp1012, yanjunchi}@sjtu.edu.cn

{weinan, leiwu}@math.pku.edu.cn

Abstract

Transformers consist of diverse building blocks, such as embedding layers, normalization layers, self-attention mechanisms, and point-wise feedforward networks. Thus, understanding the differences and interactions among these blocks is important. In this paper, we uncover a clear **sharpness disparity** across these blocks, which emerges early in training and intriguingly persists throughout the training process. Motivated by this finding, we propose **Blockwise Learning Rate (LR)**, a strategy that tailors the LR to each block’s sharpness, accelerating large language model (LLM) pre-training. By integrating Blockwise LR into AdamW, we consistently achieve lower terminal loss and nearly $2\times$ speedup compared to vanilla AdamW. We demonstrate this acceleration across GPT-2 and LLaMA, with model sizes ranging from 0.12B to 1.1B and datasets of OpenWebText and MiniPile. Finally, we incorporate Blockwise LR into Adam-mini (Zhang et al., 2024c), a recently proposed memory-efficient variant of Adam, achieving a combined $2\times$ speedup and $2\times$ memory saving. These results underscore the potential of exploiting the sharpness disparity to improve LLM training.

1 Introduction

Transformers (Vaswani et al., 2017) have achieved remarkable success across fields, including natural language processing (Brown et al., 2020), vision (Dosovitskiy et al., 2020), and scientific computing (Jumper et al., 2021). They have become the de facto design in modern AI models (Team et al., 2023; Achiam et al., 2023; Liu et al., 2024a).

Compared to traditional architectures, e.g., multilayer perceptrons (MLPs), convolutional neural networks (CNNs), and recurrent neural networks (RNNs), transformers exhibit distinctive **alloy-like characteristics**, where **diverse types of blocks** synergistically combine to achieve superior performance. A transformer at minimum includes self-attention (further broken down into query-key (QK) and value-output (VO)) blocks, point-wise feedforward networks (FFN), normalization layers (Norm), and embedding layers (Emb). Uncovering the distinct properties of these blocks, as well as the differences and interactions among them, is thus crucial for gaining a deeper insight into transformer models (Wang et al., 2024b).

* Equal contributions.

Correspondence to: Mingze Wang and Lei Wu.

In practice, transformers are typically trained using the AdamW optimizer (Kingma and Ba, 2014; Loshchilov and Hutter, 2017). Dissecting the alloy-like characteristics of transformers can provide insights into why Adam outperforms stochastic gradient descent (SGD) for transformer training (Devlin, 2018; Zhang et al., 2020; Pesme and Flammarion, 2023; Kunstner et al., 2024; Zhang et al., 2024b) and even holds promise for unlocking further improvements in training efficiency (Popel and Bojar, 2018; Xiong et al., 2020; Zhang et al., 2024c). Particularly, Zhang et al. (2024b) and Zhang et al. (2024c) observed that unlike MLPs and CNNs, the Hessian (aka sharpness or curvature) of transformers exhibits a distinct blockwise heterogeneity. Building on this insight, Zhang et al. (2024c) successfully reduced Adam’s memory footprint nearly by half without sacrificing training efficiency for a variety of LLM and non-LLM training tasks.

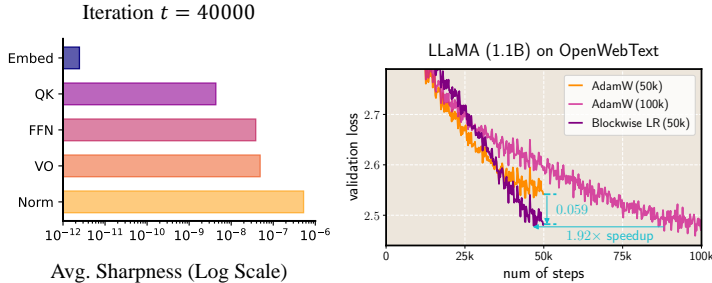


Figure 1: (left) Sharpness disparity among block types in a pre-trained GPT-2 (small), exhibiting a clear order relationship as characterized by **Principle (1)**. (right) For the pre-training of LLaMA (1.1B) on OpenWebText, incorporating our Blockwise LR strategy into AdamW results in a lower terminal loss and a $1.92\times$ speedup compared to the well-tuned vanilla AdamW.

Our Contribution. In this work, we aim to explore how we can leverage the aforementioned alloy-like characteristics of transformers to improve training efficiency. Specifically, our contributions can be summarized as follows:

- **The sharpness disparity principle.** Motivated by the alloy-like characteristics, we examine the sharpness of transformers at the level of block type. Surprisingly, we discover a distinct disparity in sharpness across different block types, summarized as follows:

$$\mathcal{S}(\text{Emb}) \ll \mathcal{S}(\text{QK}) < \mathcal{S}(\text{FFN}) < \mathcal{S}(\text{VO}) \ll \mathcal{S}(\text{Norm}) \quad (1)$$

Here $\mathcal{S}(\bullet)$ denotes the average sharpness of block type \bullet (see Eq.(4) for the calculation details). See Figure 1 (left) for an illustration of this principle. Intriguingly, this principle emerges in the early training stage and persists throughout the subsequent training process, as shown in Figure 3. These findings are validated through extensive experiments on the training of GPT-2 (Radford et al., 2019) and LLaMA models (Touvron et al., 2023), spanning various model sizes and datasets. We also provide preliminary theoretical explanations to complement these empirical observations.

- **The Blockwise LR strategy.** Inspired by **Principle (1)**, we propose tuning LR by block type to accelerate LLM pre-training. Specifically, we adjust the LR of blocks within the same type in proportion to their sharpness, while keeping the LR of the block type with the highest sharpness unchanged. This strategy accelerates the dynamics along low-sharpness directions without compromising training stability, as the latter is governed by the high-sharpness directions.

The effectiveness of Blockwise LR is extensively validated in LLM pre-training across both GPT-2 and LLaMA models, with model sizes ranging from 0.12B to 1.1B parameters, and datasets including OpenWebText (Gokaslan and Cohen, 2019) and MiniPile (Kaddour, 2023). The results can be summarized as follows:

AdamW with Blockwise LR achieves lower terminal loss
and is nearly $2\times$ **faster** than vanilla AdamW.

See Figure 1 (right) for a quick view of the acceleration effect achieved by Blockwise LR. Furthermore, we explore the compatibility of Blockwise LR with other Adam-based optimizers. Specifically, we integrate our Blockwise LR into Adam-mini (Zhang et al., 2024c), achieving both $2\times$ speedup and $2\times$ memory saving.

Remark 1.1. There has been a long-standing effort in deep learning to accelerate neural network training by adapting layerwise learning rates, a strategy that has proven effective in architectures such as MLPs and CNNs (Yang, 2019; Yang et al., 2022; Everett et al., 2024; Shin et al., 2024). However, these approaches have not been successfully transferred to the training of deep transformers. We hypothesize that this gap stems from transformers’ distinctive alloy-like characteristics: the inherent block-level diversity makes layerwise learning rate strategies inadequate. To investigate this further, we examine layer-level sharpness in Figure 7 and no clear trends emerge across layers. This suggests that while sharpness disparity exists at the block-type level, it does not exhibit a consistent pattern at the layer level.

2 Related Works

Sharpness structures in transformers. Recent work has started to investigate blockwise sharpness patterns in transformer models through Hessian-based analyses. For example, Zhang et al. (2024b) empirically observed the sharpness’ blockwise heterogeneity but did not establish a clear principle regarding the sharpness disparity among different blocks. Meanwhile, Ormaniec et al. (2024) provided a Hessian analysis for a single self-attention (SA) layer, focusing only on the sharpness disparity between the query-key (QK) and value-output (VO) blocks within the same layer.

In contrast, we examine sharpness at the block-type level across the entire transformer architecture, rather than focusing on individual blocks (as in Zhang et al. (2024b)) or a single layer (as in Ormaniec et al. (2024)). This coarse-grained perspective reveals a consistent disparity, as formalized by **Principle (1)**, which persists throughout most of the training process—except during the initial steps.

Efficient optimizers for LLM pre-training. AdamW (Adam with decoupled weight decay) (Loshchilov and Hutter, 2017) has become the default optimizer in LLM pre-training. Efforts to design more efficient optimizers generally fall into two main categories: accelerating convergence and reducing memory footprint. Accelerations have been developed using techniques such as Nesterov momentum (Xie et al., 2022), diagonal second-order estimates (Liu et al., 2024b; Wang et al., 2024a), variance reduction (Yuan et al., 2024), and matrix-based preconditioners (Keller et al., 2024; Vyas et al., 2024). Memory-efficient optimizers utilize sign-based methods (Chen et al., 2024), reduced usage of second moments in Adam (Zhang et al., 2024c), and gradient low-rank projection (Zhao et al., 2024). The closest work to our Blockwise LR is Wang et al. (2024a), which also increases the LR along low-sharpness directions. A detailed comparison is deferred to Section 5.

The edge of stability (EoS) phenomenon. Neural network training typically occurs at the EoS stage (Wu et al., 2018; Jastrzebski et al., 2020; Cohen et al., 2021; 2022), where the optimizer exhibits oscillatory behavior along sharp directions without diverging, while steadily progressing along flat directions, leading to loss reduction. Several works (Wen et al., 2024; Song et al., 2024; Cohen et al., 2024; Wang et al., 2024a) have highlighted the crucial role of the dynamics along flat directions (referred to as river directions by Wen et al. (2024), bulk directions by Song et al. (2024), and stable direction in Wang et al. (2024a)) in reducing total loss. Notably, Wen et al. (2024) further demonstrated that this picture is essential for understanding LLM pre-training. Building on these insights, our Blockwise LR approach is designed to accelerate training by amplifying the dynamics particularly along the flat river directions.

3 Preliminaries

Notations. Let $\|\cdot\|_2$, $\|\cdot\|_F$, and $\text{Tr}(\cdot)$ denote the spectral norm, Frobenius norm and trace for matrices, respectively. Given $\mathbf{A} \in \mathbb{R}^{m \times n}$, its row-wise vectorization is defined as $\text{vec}(\mathbf{A}) = (a_{1,1}, \dots, a_{1,n}, \dots, a_{m,1}, \dots, a_{m,n}) \in \mathbb{R}^{mn}$. The Kronecker product and Hadamard product are denoted by \otimes and \odot , respectively. The row-wise mean and covariance of $\mathbf{A} \in \mathbb{R}^{m \times n}$ are denoted by $\mathbb{E}_r[\mathbf{A}] \in \mathbb{R}^{m \times n}$ and $\mathbb{V}_r[\mathbf{A}] \in \mathbb{R}^{m \times n}$, respectively. Specifically, they are defined as: for all $i \in [m], j \in [n]$, $(\mathbb{E}_r[\mathbf{A}])_{i,j} = \frac{1}{n} \sum_{k=1}^n A_{i,k}$, $(\mathbb{V}_r[\mathbf{A}])_{i,j} = (A_{i,j} - \frac{1}{n} \sum_{k=1}^n A_{i,k})^2$. We will use standard big-O notations like $\mathcal{O}(\cdot)$, $\Omega(\cdot)$, and $\Theta(\cdot)$ to hide problem-independent constants.

Jacobian matrix. Given a vector-valued function: $\mathbf{b} \mapsto \mathbf{a}(\mathbf{b})$ with $\mathbf{b} \in \mathbb{R}^n$ and $\mathbf{a}(\mathbf{b}) \in \mathbb{R}^m$, the Jacobian is defined as $\frac{\partial \mathbf{a}}{\partial \mathbf{b}} = (\frac{\partial a_i}{\partial b_j})_{i,j} \in \mathbb{R}^{m \times n}$. Analogously, for a matrix-valued function:

$B \mapsto A(B)$ where $B \in \mathbb{R}^{p \times q}$ and $A(B) \in \mathbb{R}^{m \times n}$, to avoid directly working with tensors, the Jacobian is defined as $\frac{\partial A}{\partial B} := \frac{\partial \text{vec}(A)}{\partial \text{vec}(B)} \in \mathbb{R}^{mn \times pq}$.

3.1 The Transformer Architecture

Given an n -token input sequence $\mathbf{X} = (\mathbf{x}_1^\top, \dots, \mathbf{x}_n^\top)^\top \in \mathbb{R}^{n \times d}$, where d refers to the vocabulary size in LLM and each \mathbf{x}_i corresponds to the token's one-hot encoding, an L -layer transformer TF processes it as follows.

Embedding layer. First, each input token is embedded into the latent space through an embedding layer with parameters $\mathbf{W}_E \in \mathbb{R}^{d \times D}$, $\mathbf{b}_E \in \mathbb{R}^{1 \times D}$:

$$\mathbf{x}_s^{(0)} = \mathbf{x}_s \mathbf{W}_E + \mathbf{b}_E, \quad s \in [n],$$

where the bias \mathbf{b}_E is omitted in LLMs such as nanoGPT (Karpathy, 2022).

L -layer SA-FFN blocks. Then the embedded sequence $\mathbf{X}^{(0)}$ is processed by L -layer SA-FFN blocks, and the output of the final layer is taken as the output sequence $\text{TF}(\mathbf{X}) = \mathbf{X}^{(L)} \in \mathbb{R}^{n \times D}$. For each layer $l \in [L]$, the computations are as follows:

$$\begin{aligned} \mathbf{X}^{(l-\frac{1}{2})} &= \mathbf{X}^{(l-1)} + \text{SA}^{(l)}(\text{Norm}^{(l-1/2)}(\mathbf{X}^{(l-1)})); \\ \mathbf{X}^{(l)} &= \mathbf{X}^{(l-\frac{1}{2})} + \text{FFN}^{(l)}(\text{Norm}^{(l)}(\mathbf{X}^{(l-\frac{1}{2})})). \end{aligned} \quad (2)$$

Norm blocks. Here, $\text{Norm}^{(v)}$ ($v \in \{l-1/2, l\}$) denote normalization layers (e.g., LayerNorm (Lei Ba et al., 2016) and RMSNorm (Zhang and Sennrich, 2019)) with learnable parameters $\gamma^{(v)}, \beta^{(v)} \in \mathbb{R}^{1 \times D}$. For LayerNorm, the computation for a token $\mathbf{x} \in \mathbb{R}^{1 \times D}$ is:

$$\text{Norm}^{(v)}(\mathbf{x}) = \frac{\mathbf{x} - \mathbb{E}_r[\mathbf{x}]}{\sqrt{\mathbb{V}_r[\mathbf{x}]}} \odot \gamma^{(v)} + \beta^{(v)}.$$

where the bias β is omitted in LLMs such as nanoGPT.

FFN blocks. $\text{FFN}^{(l)}$ denotes a (token-wise) two-layer FFN of width M , comprising parameters $\mathbf{W}_1^{(l)} \in \mathbb{R}^{D \times M}$, $\mathbf{W}_2^{(l)} \in \mathbb{R}^{M \times D}$, and using activation function $\sigma(\cdot)$ such as ReLU. For any token $\mathbf{x} \in \mathbb{R}^{1 \times D}$, the operation is:

$$\text{FFN}^{(l)}(\mathbf{x}) = \sigma(\mathbf{x} \mathbf{W}_1^{(l)}) \mathbf{W}_2^{(l)}.$$

SA blocks. $\text{SA}^{(l)}$, a multi-head self-attention, has parameters $\mathbf{W}_Q^{(l)}, \mathbf{W}_K^{(l)}, \mathbf{W}_V^{(l)}, \mathbf{W}_O^{(l)} \in \mathbb{R}^{D \times D}$. When applied to a sequence $\mathbf{Z} \in \mathbb{R}^{n \times D}$, it operates as:

$$\begin{aligned} \text{SA}^{(l)}(\mathbf{Z}) &= \sum_{h=1}^H \text{SA}^{(l,h)}(\mathbf{Z}) \mathbf{W}_O^{(l,h)}, \quad \text{SA}^{(l,h)}(\mathbf{Z}) = \\ &\text{softmax} \left(\frac{\left\langle \mathbf{Z} \mathbf{W}_Q^{(l,h)}, \mathbf{Z} \mathbf{W}_K^{(l,h)} \right\rangle + M}{\sqrt{D/H}} \right) \left(\mathbf{Z} \mathbf{W}_V^{(l,h)} \right), \end{aligned}$$

where H is the head number, and $\mathbf{W}_Q^{(l,h)}, \mathbf{W}_K^{(l,h)}, \mathbf{W}_V^{(l,h)} \in \mathbb{R}^{D \times (D/H)}$, $\mathbf{W}_O^{(l,h)} \in \mathbb{R}^{(D/H) \times D}$ are split from $\mathbf{W}_Q^{(l)}, \mathbf{W}_K^{(l)}, \mathbf{W}_V^{(l)}, \mathbf{W}_O^{(l)}$ by heads, respectively. The operator $\text{softmax}(\cdot)$ represents the row-wise softmax normalization. For the next-token prediction, the mask $\mathbf{M} \in \mathbb{R}^{n \times n}$ satisfies $M_{i,j} = -\infty$ if $i < j$ and $M_{i,j} = 0$ otherwise.

3.2 Blockwise Sharpness and the Efficient Estimation

Measuring sharpness requires accessing the Hessian matrix, which is computationally expensive due to the high dimensionality of the parameter space. Consequently, approximate methods are needed to reduce computational complexity.

Let $\ell(\cdot, \cdot)$ denote the cross-entropy loss. For an input data $\mathbf{x} \in \mathbb{R}^{d_x}$ and label $\mathbf{y} \in \mathbb{R}^{d_y}$, let the model's prediction be $f(\mathbf{x}; \boldsymbol{\theta}) \in \mathbb{R}^{d_y}$. The Fisher (Gauss-Newton) matrix $F(\boldsymbol{\theta})$ is widely recognized approximation of the Hessian, particularly near minima. Thus, the diagonal Hessian can be estimated as $\mathbf{h}(\boldsymbol{\theta}) = \text{diag}(F(\boldsymbol{\theta}))$, a popular technique in deep learning optimization (Martens and Grosse, 2015;

Grosse and Martens, 2016; George et al., 2018; Mi et al., 2022; Liu et al., 2024b; Wang et al., 2024a). Moreover, given an input batch $\{(\mathbf{x}_b, \mathbf{y}_b)\}_{b=1}^B$, the empirical diagonal Fisher can be estimated: $\text{diag}(\hat{F}(\boldsymbol{\theta})) = \frac{1}{B} \sum_{b=1}^B \nabla \ell(f(\mathbf{x}_b; \boldsymbol{\theta}); \hat{\mathbf{y}}_b) \odot \nabla \ell(f(\mathbf{x}_b; \boldsymbol{\theta}); \hat{\mathbf{y}}_b)$, where $\hat{\mathbf{y}}_b \sim \text{softmax}(f(\boldsymbol{\theta}; \mathbf{x}_b))$. However, as noted by Liu et al. (2024b), implementing this estimator is computationally expensive due to the need to calculate B single-batch gradients. Liu et al. (2024b) proposed a more convenient estimator $\text{diag}(\hat{F}_{\text{eff}}(\boldsymbol{\theta}))$, which only requires the computation of the mini-batch gradient $\nabla \hat{\mathcal{L}}_B(\boldsymbol{\theta}) = \frac{1}{B} \sum_{b=1}^B \nabla \ell(f(\mathbf{x}_b; \boldsymbol{\theta}); \hat{\mathbf{y}}_b)$ with $\hat{\mathbf{y}}_b \sim \text{softmax}(f(\mathbf{x}_b; \boldsymbol{\theta}))$:

$$\mathbf{h}(\boldsymbol{\theta}) = \text{diag}(\hat{F}_{\text{eff}}(\boldsymbol{\theta})) = B \cdot \nabla \hat{\mathcal{L}}_B(\boldsymbol{\theta}) \odot \nabla \hat{\mathcal{L}}_B(\boldsymbol{\theta}). \quad (3)$$

According to Liu et al. (2024b, Section 2), this estimator is unbiased, i.e., $\mathbb{E}_{\hat{\mathbf{y}}_b}[\text{diag}(\hat{F}_{\text{eff}}(\boldsymbol{\theta}))] = \mathbb{E}_{\hat{\mathbf{y}}_b}[\text{diag}(\hat{F}(\boldsymbol{\theta}))]$.

Given a block type $\bullet \in \{\text{Emb}, \text{QK}, \text{VO}, \text{FFN}, \text{Norm}\}$, let $\boldsymbol{\theta}[\bullet]$ represent the parameters associated with all blocks of that type, and let $\mathbf{h}(\boldsymbol{\theta}[\bullet])$ denote the corresponding diagonal Hessian. The average sharpness for each block type can then be approximated as follows:

$$S(\boldsymbol{\theta}[\bullet]) := \frac{\text{Tr}(\mathbf{h}(\boldsymbol{\theta}[\bullet]))}{\#(\boldsymbol{\theta}[\bullet])} = \frac{B \left\| \nabla_{\boldsymbol{\theta}[\bullet]} \hat{\mathcal{L}}_B(\boldsymbol{\theta}) \right\|_{\text{F}}^2}{\#(\boldsymbol{\theta}[\bullet])}, \quad (4)$$

where $\hat{\mathcal{L}}_B$ corresponds to (3) and $\#(\boldsymbol{\theta}[\bullet])$ denotes the number of parameters associated with the block type \bullet . For brevity, $\boldsymbol{\theta}$ in (4) will be omitted when there is no ambiguity.

Remark 3.1. It is worth noting that in (4), the sharpness is averaged over all blocks of the same type, which may be distributed across different layers, rather than being calculated within each individual block.

4 The Sharpness Disparity Principle

4.1 Main Findings

We first investigate the sharpness disparity across different types of building blocks (Emb, QK, VO, FFN, Norm) in transformer-based LLMs. Specifically, we pre-trained GPT-2 (Radford et al., 2019) and LLaMA (Touvron et al., 2023) models on the OpenWebText dataset using default configurations. Blockwise diagonal Hessians are analyzed at various checkpoints using the Hessian estimator (3). The experimental details can be found in Appendix A.1.

In Figures 1 (left) and 2 (left), we report the average sharpness, estimated using (4), of the five typical types of blocks for GPT-2 and LLaMA, respectively. The results reveal a clear and consistent sharpness disparity among different block types, as summarized in **Principle (1)**. Specifically, Norm layers consistently exhibit the highest sharpness, the Emb layers are the flattest, and QK layers are relatively flatter compared to FFN and VO layers. These findings, to the best of our knowledge, provide the first comprehensive comparison of sharpness across block types in transformers.

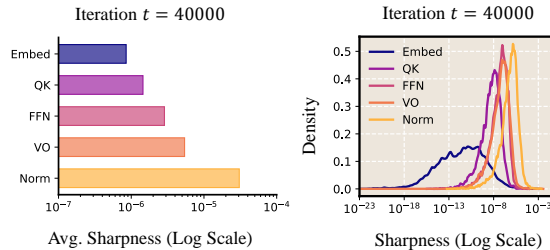
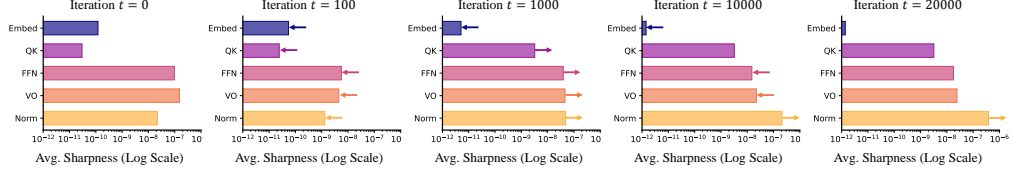
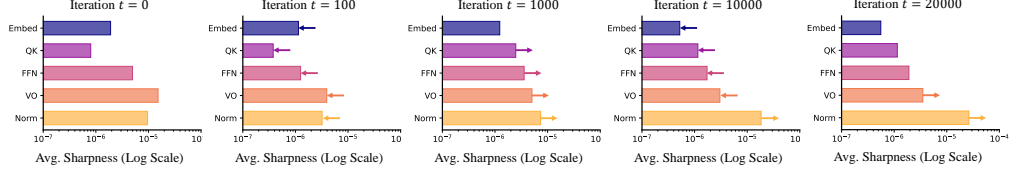


Figure 2: (left) The average sharpness for the five typical block types in a pre-trained LLaMA model (0.25B); (right) the sharpness distribution across different blocks in a pre-trained GPT-2 (small) model.

Figure 2 (right) plots the full sharpness distribution for each block type, whereas Figures 1 (left) and 2 (left) only report mean sharpness values. Evidently, even at the distribution level, **Principle (1)** remains valid. Interestingly, the Emb block exhibits much higher variance compared to other blocks.



(a) Evolution of the average sharpness across different blocks during pre-training GPT-2 (small) on OpenWebText.



(b) Evolution of the average sharpness across different blocks during pre-training LLaMA (0.25B) on OpenWebText.

Figure 3: In these experiments, the total training steps are both 50k. **Principle (1)** emerges during the initial phase (from iteration 0 to iteration 1k), which accounts for only approximately 2% of the total steps, and persists throughout the subsequent training process.

This behavior likely stems from the embedding layer’s direct interaction with the entire vocabulary, where rare tokens result in the wide spread of small sharpness and frequent tokens contribute to large sharpness. A similar insight has been utilized by [Kunstner et al. \(2024\)](#) to explain the necessity of Adam in training NLP models.

Furthermore, Figure 3 illustrates the evolution of blockwise sharpness during the training process. We can see that **Principle (1)** is not exclusive to well-trained transformers; instead, it emerges in the early stages of training and persists consistently throughout the subsequent training process. This observation underscores the potential of leveraging **Principle (1)** to enhance LLM pre-training; we refer to Section 5 for further explorations.

Comparison with existing works. Our findings build on prior work, extending key observations. [Zhang et al. \(2024b\)](#) noted the block heterogeneity in the Hessian of transformers but did not establish a clear principle for sharpness distinctions across blocks, as we do with **Principle (1)**. The work of [Ormaniec et al. \(2024\)](#) is more closely related but focuses solely on a single self-attention layer (SA), reporting the relationship $\mathcal{S}(\text{QK}) < \mathcal{S}(\text{VO})$. In contrast, we analyze all major block types in transformers, including Emb, FFN, and Norm, thereby offering a more comprehensive principle that captures the full scope of sharpness disparity.

4.2 Theoretical Insights

To provide theoretical insights into explaining **Principle (1)**, we derive analytic expressions of $\mathcal{S}(\bullet)$ and analyze their dependence on parameter magnitudes and numbers of each block. For simplicity, we denote $\mathcal{Q}(\theta) := \hat{\mathcal{L}}_B(\theta)$, where $\hat{\mathcal{L}}_B(\theta)$ is defined in (3). Then from (4), we have $\mathcal{S}(\bullet) = B \|\nabla_{\bullet} \mathcal{Q}\|_F^2 / \#(\bullet)$. Without loss of generality, we set $B = 1$. Our calculations for $\nabla \mathcal{Q}$ apply to general \mathcal{Q} .

Considering blocks across different layers is complicated. Therefore, we focus on comparisons within the same layer. Specifically, we examine the following sharpness comparisons: (i) FFN vs. Norm within the same layer; (ii) SA (comprising QK and VO) vs. Norm within the same layer; and (iii) Emb vs. the adjacent Norm.

Theorem 4.1 (FFN vs. Norm). *Consider the l -th layer in a transformer (2). Omitting the layer index for simplicity, let $\mathbf{Y} = \mathbf{X} + \text{FFN}(\text{Norm}(\mathbf{X}; \gamma); \mathbf{W}_1, \mathbf{W}_2)$, where FFN utilizes the (Leaky) ReLU activation σ . Then, the gradients of \mathcal{Q} w.r.t. \mathbf{W}_1 , \mathbf{W}_2 , and γ are:*

$$\frac{\partial \mathcal{Q}}{\partial \mathbf{W}_2} = \frac{\partial \mathcal{Q}}{\partial \mathbf{Y}} \left(\mathbf{X}_{\text{Norm}} \mathbf{W}_1 \odot \frac{\partial \mathbf{A}}{\partial \mathbf{M}} \right) \otimes \mathbf{I}_d;$$

$$\begin{aligned}\frac{\partial \mathcal{Q}}{\partial \mathbf{W}_1} &= \frac{\partial \mathcal{Q}}{\partial \mathbf{Y}} \left(\mathbf{I}_n \otimes \mathbf{W}_2^\top \right) \frac{\partial \mathbf{A}}{\partial \mathbf{M}} \left(\mathbf{X}_{\text{Norm}} \otimes \mathbf{I}_M \right); \\ \frac{\partial \mathcal{Q}}{\partial \gamma} &= \frac{\partial \mathcal{Q}}{\partial \mathbf{Y}} \left(\mathbf{I}_n \otimes \mathbf{W}_2^\top \right) \frac{\partial \mathbf{A}}{\partial \mathbf{M}} \left(\mathbf{I}_n \otimes \mathbf{W}_1^\top \right) \\ &\quad \text{diag}(\text{vec}(\mathbf{X}_{\text{std}})) (\mathbf{1}_{n \times 1} \otimes \mathbf{I}_d),\end{aligned}$$

where $\mathbf{X}_{\text{std}} := \frac{\mathbf{X} - \mathbb{E}_r[\mathbf{X}]}{\sqrt{\text{Var}[\mathbf{X}]}}$, $\mathbf{X}_{\text{Norm}} := \text{Norm}(\mathbf{X}; \gamma) = \mathbf{X}_{\text{std}} \odot (\mathbf{1}_{n \times 1} \otimes \gamma)$, $\mathbf{A} := \sigma(\mathbf{M})$, $\mathbf{M} := \mathbf{X}_{\text{Norm}} \mathbf{W}_1$. Let $\Psi := n\sqrt{D} \left\| \frac{\partial \mathcal{Q}}{\partial \mathbf{Y}} \right\|_{\text{F}} \left\| \frac{\partial \mathbf{A}}{\partial \mathbf{M}} \right\|_{\text{F}} \|\mathbf{W}_1\|_{\text{F}} \|\mathbf{W}_2\|_{\text{F}} \|\gamma\|_{\text{F}}$. Then, the blockwise average sharpness can be bounded as:

$$\begin{aligned}\mathcal{S}(\mathbf{W}_\bullet) &= \mathcal{O} \left(\frac{\Psi^2}{D^2 \|\mathbf{W}_\bullet\|_{\text{F}}^2} \right), \bullet \in \{1, 2\}; \\ \mathcal{S}(\gamma) &= \mathcal{O} \left(\frac{\Psi^2}{D \|\gamma\|_{\text{F}}^2} \right),\end{aligned}$$

where the denominators (D^2 or D) reflect the number of parameters in each group.

Theorem 4.1 provides theoretical support for our main finding: $\mathcal{S}(\text{FFN})$ is substantially smaller than $\mathcal{S}(\text{Norm})$. As illustrated in Figure 6 (a), during training, $\|\gamma\|_{\text{F}}$ gradually decreases, and $\|\mathbf{W}_\bullet\|_{\text{F}}$ ($\bullet \in \{1, 2\}$) in FFN layers remains larger than $\|\gamma\|_{\text{F}}$, resulting in $D^2 \|\mathbf{W}_\bullet\|_{\text{F}}^2 \gg D \|\gamma\|_{\text{F}}^2$.

Theorem 4.2 (QK, VO vs. Norm). Consider the $(l - \frac{1}{2})$ -th layer in (2). Omitting the layer index for simplicity, let $\mathbf{Y} = \mathbf{X} + \text{SA}(\text{Norm}(\mathbf{X}; \gamma); \mathbf{W}_K, \mathbf{W}_Q, \mathbf{W}_V, \mathbf{W}_O)$. Consider a single-head attention (i.e., $H = 1$) for simplicity. Then, the gradients of \mathcal{Q} w.r.t. different blocks ($\mathbf{W}_K, \mathbf{W}_Q, \mathbf{W}_V, \mathbf{W}_O, \gamma$) are provided in Appendix B.2. Furthermore, there exist two problem-dependent constants $\Phi, \Psi > 0$ (detailed in Appendix B.2), such that:

$$\begin{aligned}\mathcal{S}(\mathbf{W}_\bullet) &= \mathcal{O} \left(\frac{\Phi^2}{D^2 \|\mathbf{W}_\bullet\|_{\text{F}}^2} \right), \bullet \in \{K, Q\}; \\ \mathcal{S}(\mathbf{W}_\bullet) &= \mathcal{O} \left(\frac{\Psi^2}{D^2 \|\mathbf{W}_\bullet\|_{\text{F}}^2} \right), \bullet \in \{V, O\}; \\ \mathcal{S}(\gamma) &= \mathcal{O} \left(\frac{\Phi^2 + \Psi^2}{D \|\gamma\|_{\text{F}}^2} \right).\end{aligned}$$

where the denominators (D^2 or D) reflect the number of parameters in each group.

Theorem 4.2 provides theoretical support for our main finding that both $\mathcal{S}(\text{QK})$ and $\mathcal{S}(\text{VO})$ are significantly smaller than $\mathcal{S}(\text{Norm})$. The inclusion of the softmax operation in attention layers introduces additional complexity in the calculations. Detailed derivations are given in the appendix. As shown in Figure 6 (b), during training, $\|\gamma\|_{\text{F}}$ gradually decreases, and $\|\mathbf{W}_\bullet\|_{\text{F}}$ ($\bullet \in \{K, Q, V, O\}$) in SA blocks remains larger than $\|\gamma\|_{\text{F}}$, resulting in $D^2 \|\mathbf{W}_\bullet\|_{\text{F}}^2 \gg D \|\gamma\|_{\text{F}}^2$.

This theorem does not explicitly establish that $\mathcal{S}(\text{QK}) < \mathcal{S}(\text{VO})$. Studying this relation requires a deeper analysis of the constants Φ and Ψ , as well as the magnitudes of $\|\mathbf{W}_\bullet\|_{\text{F}}$. Ormaniec et al. (2024) has demonstrated $\mathcal{S}(\text{QK}) < \mathcal{S}(\text{VO})$ both theoretically and experimentally, and we defer to that analysis instead of repeating it here.

Theorem 4.3 (Emb v.s. Norm). Consider the embedding layer and its adjoint normalization layer of a transformer (2). Omitting the layer index for simplicity, let: $\mathbf{Y} := \text{Norm}(\mathbf{X} \mathbf{W}_{\text{emb}}; \gamma)$. The gradients of \mathcal{Q} w.r.t \mathbf{W}_{emb} and γ are derived in Appendix B.3. Moreover, there exists a problem-dependent constant $\Psi > 0$ (also detailed in Appendix B.3), such that:

$$\begin{aligned}\mathcal{S}(\mathbf{W}_E) &= \mathcal{O} \left(\frac{\Psi^2}{D d \min_{i \in [d]} \|\tilde{\mathbf{w}}_{E_i}\|_2^2} \right); \\ \mathcal{S}(\gamma) &= \mathcal{O} \left(\frac{\Psi^2}{D \|\gamma\|_{\text{F}}^2} \right),\end{aligned}$$

where $\tilde{\mathbf{W}}_E = (\tilde{\mathbf{w}}_{E_1}^\top, \dots, \tilde{\mathbf{w}}_{E_d}^\top)^\top := \mathbf{W}_E - \mathbb{E}_r[\mathbf{W}_E]$. The denominators (Dd or D) represent the number of parameters in each group.

Theorem 4.3 provides theoretical justification for our main finding that $\mathcal{S}(\text{Emb})$ is much smaller than $\mathcal{S}(\text{Norm})$. As shown in Figure 6(c), during training, $Dd \|\tilde{\mathbf{w}}_{E_i}\|_2^2 \gg D \|\gamma\|_F^2$. (Notice that the vocabulary size d is very large in practice, e.g., 50304 for the GPT tokenizer.)

Recalling the definition of average sharpness (4), the key step in deriving Theorem 4.1 and 4.2, and 4.3 is establishing $\|\nabla_{\bullet} \mathcal{Q}\| = \mathcal{O}(1/\|\theta[\bullet]\|)$. This relationship is highly intuitive given the compound multiplicative nature of transformer blocks, where the norm of the derivatives is inversely proportional to the norm of associated parameters, even with weak non-linearities. For example, if $y = \prod_{i=1}^n x_i$ and $\mathcal{Q} = \varphi(y)$, then $|\partial \mathcal{Q} / \partial x_i| = |\phi'(y)y/x_i| \propto 1/|x_i|$ for all $i \in [n]$.

5 The Blockwise LR Strategy

Recalling Figure 3, the sharpness disparity across different blocks, as described in (1), emerges early in training and persists until convergence. This insight can be leveraged to accelerate LLM pre-training, as elaborated later.

Fast-slow dynamics at EoS. As discussed in Section 2, recent studies (Wen et al., 2024; Song et al., 2024; Wang et al., 2024a) have highlighted the distinct roles of the dynamics along high- and low-sharpness directions during EoS. The main picture is summarized as follows:

- **Fast dynamics:** Along *high-sharpness directions*, the optimizer exhibits significant fluctuations without converging or diverging. These components of dynamics govern training stability, as further increasing the LR in these directions can lead to instability, while contributing little to loss reduction.
- **Slow dynamics:** Along *low-sharpness directions*, the optimizer progresses steadily, making the primary contribution to loss reduction, albeit at a slow rate.

Inspired by the above picture, a promising approach to accelerating training is as follows: given a base optimizer, increase the LRs along low-sharpness directions while keeping the LR of high-sharpness directions unchanged. This strategy aims to speed up loss reduction without compromising training stability.

Wang et al. (2024a) has implemented this idea by adjusting the LR of each parameter based on its sharpness. However, this approach faces two key challenges: 1) it requires frequent diagonal Hessian estimation, which imposes significant computational and memory overhead; 2) sharpness estimates at the individual parameter level can be unreliable.

The Blockwise LR. Unlike Wang et al. (2024a), we propose adjusting LRs at the block-type level, as our **Principle (1)** reveals a consistent sharpness disparity at this granularity. Specifically, let η_{base} denote the LR for base optimizers such as AdamW, the LR for each block type is then adjusted as follows:

- Norm blocks (the sharpest directions): we still use the base LR, $\eta_{\text{Norm}} = \eta_{\text{base}}$, to keep training stability;
- Other blocks (low-sharpness directions): we adjust the LRs of these blocks by $\eta_{\bullet} \propto r(\bullet)\eta_{\text{base}}$, where $\bullet \in \{\text{Emb}, \text{QK}, \text{FFN}, \text{VO}\}$, where $r(\bullet)$ denotes the adjusting ratio for the block type \bullet .

Naturally, we can set $r(\bullet) \propto \mathcal{S}(\text{Norm})/\mathcal{S}(\bullet)$. However, in practice, we find that manually tuning $r(\bullet)$'s—involving only four hyperparameters—while following the qualitative trend described by **Principle (1)** is more effective. Further details are provided in Section 6.

It is also worth noting that due to its simplicity, Blockwise LR can be seamlessly integrated into modern LLM training frameworks such as Megatron (Shoeybi et al., 2019).

6 Experiments

Models and datasets. We evaluate our proposed Blockwise LR in the pre-training of decoder-only LLMs across various model types, model sizes, and datasets. Specifically, we consider two widely-used LLMs: **LLaMA** and **GPT-2**; we experiment with model sizes ranging from **0.12B** to **1.1B**

parameters; the datasets includes OpenWebText (Gokaslan and Cohen, 2019)¹ and MiniPile (Kaddour, 2023)².

Baselines. As a baseline, we use the default AdamW optimizer, configured with the hyperparameters $\beta_1 = 0.9, \beta_2 = 0.95$ and weight decay $\lambda = 0.1$. To ensure training stability, gradient clipping is applied with 1.0. These settings align with the training protocols used in nanoGPT and LLaMA models (Touvron et al., 2023). The LR strategy includes a linear warm-up phase followed by a cosine decay scheduler, capped at lr_max . And the terminal LR lr_min is set to $\text{lr_max}/20$. For each experiment, we *first tune* the lr_max to be optimal for AdamW, and the baselines are trained using these optimal lr_max 's. Details of the tuned lr_max values can be found in Appendix A.1.

Adjusting ratio tuning and its transferability. To incorporate the Blockwise LR into AdamW, we simply use the lr_max (tuned for vanilla AdamW) for NORM blocks. Then, we **only tuned the four adjusting ratios in a single small-scale experiment** – specifically the pre-training of LLaMA (0.25B) on Minipile – following the rule: $r(\bullet)$ is adjusted according to the trend of $\frac{S(\text{Norm})}{S(\bullet)}$, guided by **Principle (1)**. The tuned hyperparameters are:

$$r(\text{Emb}) = 10, r(\text{QK}) = 8, r(\text{FFN}) = 6, r(\text{VO}) = 4. \tag{5}$$

Notably, the adjusting ratios are highly robust hyperparameters, as demonstrated in the following ways:

- First, as shown in Figure 8, in the experiments for tuning the adjusting ratios, Blockwise LR demonstrates robustness to these hyperparameters, consistently accelerating pre-training across a range of $r(\bullet)$'s. The configuration in (5) achieves the largest improvements among those tested. Notably, even with suboptimal ratios, Blockwise LR still delivers significant performance gains. Further details are provided in Appendix A.2.
- Second, the configuration in (5), tuned from a single experiment, **transfers perfectly** across all AdamW experiments conducted in this paper. Consequently, **we adopt (5) as the default adjusting ratios for all AdamW experiments**. This robustness aligns with the consistency of **Principle (1)**, which holds across GPT and LLaMA models, various model sizes, and datasets.

6.1 Main Results

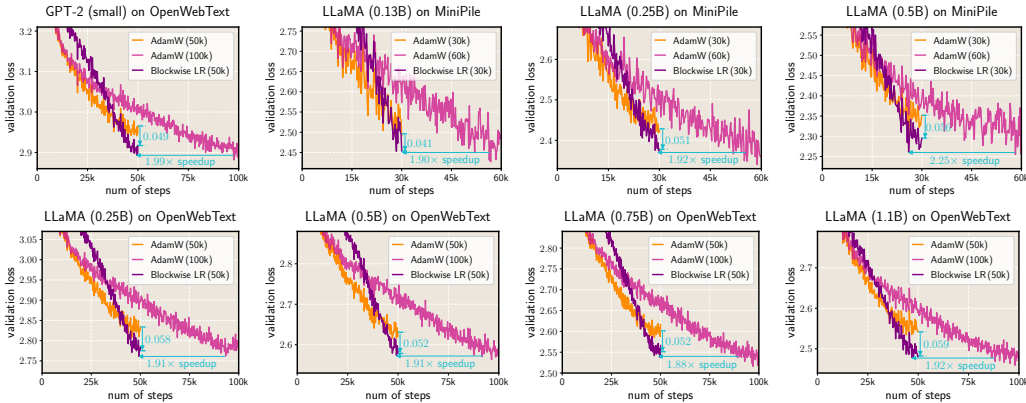


Figure 4: AdamW with Blockwise LR consistently outperforms AdamW in LLM pre-training tasks across different model types, varying model sizes, and datasets.

In Figure 4, we compare the performance of AdamW with Blockwise LR against vanilla AdamW across various settings. Our observations, which consistently hold across all experiments—including both GPT-2 and LLaMA models with sizes ranging from 0.12B to 1.1B—and datasets such as OpenWebText and MiniPile, are as follows:

¹An opensource recreation of the WebText corpus, widely used for LLM pre-training such as RoBERTa (Liu et al., 2019) and GPT-2.

²A 6GB subset of the deduplicated Pile (825GB) (Gao et al., 2020), providing a highly diverse text corpus.

- Given the same total number of training steps, Blockwise LR enables AdamW to reach a **lower terminal loss** than vanilla AdamW.
- Across different total training steps, AdamW with Blockwise LR achieves a **nearly 2× speedup** compared to vanilla AdamW.

An intriguing observation in Figure 4 is that AdamW with BlockWise LR often starts to outperform vanilla AdamW from the mid-to-late stages of training. This behavior resembles the WSD scheduler (Wen et al., 2024; Hu et al., 2024), which typically surpasses cosine or linear decay LR schedulers in the late stage (during the decay phase). Understanding the underlying cause of this phenomenon requires further investigation, which we leave for future work.

6.2 Ablation Studies

In the preceding experiments, Blockwise LR is applied to all major blocks simultaneously. Here, we conduct ablation studies to assess the contribution of each block type individually. Specifically, we pre-train a LLaMA model (0.25B) on OpenWebText focusing on three comparisons: (i) applying Blockwise LR exclusively to Emb; (ii) applying Blockwise LR to both Emb and FFN; (iii) applying Blockwise LR to blocks of all the four types (Emb, FFN, QK, and VO). The adjusting ratios follow Eq. (5) and the results are shown in Table 1.

First, the results show that applying Blockwise LR to any block consistently improves performance, supporting the hypothesis that dynamics along low-sharpness directions are crucial for loss reduction. Among all blocks, applying Blockwise LR to FFN yields the largest improvement ($0.043 - 0.016 = 0.027$), likely because FFN blocks comprise the majority of model parameters, offering the greatest potential for optimization gains.

Table 1: Ablation results for the effectiveness of Blockwise LR in pre-training LLaMA (0.25B) on OpenWebText.

| Blockwise LR | terminal loss (50k steps) |
|---------------------|---------------------------|
| w/o | 2.834 |
| Emb | 2.818 (-0.016 ✓) |
| Emb & FFN | 2.791 (-0.043 ✓) |
| Emb & FFN & QK & VO | 2.784 (-0.050 ✓) |
| Norm | 2.837 (+0.003 ✗) |

Second, we conduct an additional experiment to assess the impact of increasing the LR for Norm blocks. Specifically, the Norm LR is doubled, while the LR for other blocks remains unchanged from the baseline. As shown in the last row of Table 1, this leads to a deterioration in performance, contrasting with the improvements seen when increasing the LR for other blocks by far more than double. This result underscores a fundamental difference in the dynamics of Norm with other blocks.

In summary, these ablation studies further validate the effectiveness of Blockwise LR and confirm the rationale of selecting specific types of blocks for LR amplification, as guided by the sharpness disparity principle.

6.3 Integration into Adam-mini

In practice, there are two popular directions for improving LLM pre-training: acceleration and reducing memory consumption. While Blockwise LR has demonstrated remarkable success in accelerating pre-training, a natural **question** arises: *Can Blockwise LR be combined with memory-efficient optimizers to achieve both faster training and fewer memory consumption?*

Blockwise LR on Adam-mini. Without loss of generality, we choose the Adam-mini (Zhang et al., 2024c) optimizer, an Adam variant that reduces memory consumption by approximately 2× compared to AdamW. Here, we conduct experiments to explore whether Blockwise LR can also accelerate Adam-mini. Following Zhang et al. (2024c), we adopt the `lr_max` that tuned for AdamW as the `lr_max` of Adam-mini. However, since Adam-mini employs SGD within each block, its dynamics differs significantly from AdamW. Consequently, for Adam-mini with Blockwise LR, we re-tune the ratios $r(\bullet)$ for $\bullet \in \{\text{Emb, QK, FFN, VO}\}$. More experimental details are provided in Appendix A.3.

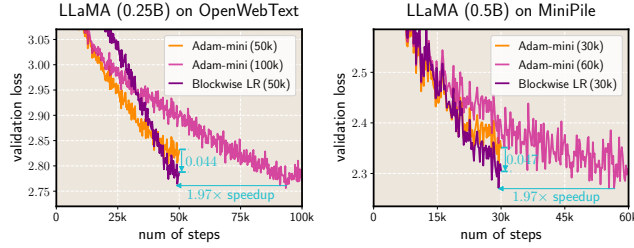


Figure 5: Adam-mini with Blockwise LR outperforms Adam-mini in pre-training tasks.

The results, presented in Figure 5, demonstrate that **Blockwise LR achieves a $2\times$ speedup on Adam-mini**. Since vanilla Adam-mini already achieves a $2\times$ memory saving compared to AdamW while maintaining nearly the same convergence speed, Adam-mini combined with Blockwise LR achieves both a $2\times$ speedup and $2\times$ memory saving compared to vanilla AdamW. We leave more ablation studies with other optimizers for future work.

This experiment demonstrates that Blockwise LR is not limited to accelerating AdamW but can also be effectively combined with other optimizers, such as Adam-mini, while preserving their unique advantages. This finding paves the way for future research exploring the integration of Blockwise LR with other optimization algorithms.

7 Conclusion and Outlook

In this paper, we uncovered a sharpness disparity principle among different types of blocks in transformers, as formalized in Eq. (1). Notably, this blockwise sharpness disparity persists throughout the entire training process, except during the initial few steps. Building on this discovery, we proposed a novel Blockwise LR adjustment principle, which effectively accelerates base optimizers such as AdamW and Adam-mini in LLM pre-training tasks.

Future works. It would be valuable to investigate the applicability of our Blockwise LR to non-LLM tasks, such as computer vision, and its compatibility with other optimizers, such as Muon (Keller et al., 2024) and other alloy-like architectures such as Mamba (Gu and Dao, 2023). Furthermore, our findings open up opportunities to develop other block-adaptive optimization strategies, such as blockwise weight decay and gradient clipping, which could further enhance training efficiency and performance.

Acknowledgments

Lei Wu is supported by the National Key R&D Program of China (No. 2022YFA1008200) and National Natural Science Foundation of China (No. 12288101). Mingze Wang is supported by Young Scientists (PhD) Fund of the National Natural Science Foundation of China (No. 124B2028).

References

- Josh Achiam, Steven Adler, Sandhini Agarwal, Lama Ahmad, Ilge Akkaya, Florencia Leoni Aleman, Diogo Almeida, Janko Altenschmidt, Sam Altman, Shyamal Anadkat, et al. GPT-4 technical report. *arXiv preprint arXiv:2303.08774*, 2023. 1
- Joshua Ainslie, James Lee-Thorp, Michiel de Jong, Yury Zemlyanskiy, Federico Lebron, and Sumit Sanghai. GQA: Training generalized multi-query transformer models from multi-head checkpoints. In Houda Bouamor, Juan Pino, and Kalika Bali, editors, *Proceedings of the 2023 Conference on Empirical Methods in Natural Language Processing*, pages 4895–4901, Singapore, December 2023. Association for Computational Linguistics. doi: 10.18653/v1/2023.emnlp-main.298. URL <https://aclanthology.org/2023.emnlp-main.298/>. 16
- Tom Brown, Benjamin Mann, Nick Ryder, Melanie Subbiah, Jared D Kaplan, Prafulla Dhariwal, Arvind Neelakantan, Pranav Shyam, Girish Sastry, Amanda Askell, et al. Language models are few-shot learners. *Advances in neural information processing systems*, 33:1877–1901, 2020. 1

- Xiangning Chen, Chen Liang, Da Huang, Esteban Real, Kaiyuan Wang, Hieu Pham, Xuanyi Dong, Thang Luong, Cho-Jui Hsieh, Yifeng Lu, et al. Symbolic discovery of optimization algorithms. *Advances in Neural Information Processing Systems*, 36, 2024. 3
- Jeremy M Cohen, Simran Kaur, Yuanzhi Li, J Zico Kolter, and Ameet Talwalkar. Gradient descent on neural networks typically occurs at the edge of stability. *International Conference on Learning Representations*, 2021. 3
- Jeremy M Cohen, Behrooz Ghorbani, Shankar Krishnan, Naman Agarwal, Sourabh Medapati, Michal Badura, Daniel Suo, David Cardoze, Zachary Nado, George E Dahl, et al. Adaptive gradient methods at the edge of stability. *arXiv preprint arXiv:2207.14484*, 2022. 3
- Jeremy M Cohen, Alex Damian, Ameet Talwalkar, Zico Kolter, and Jason D Lee. Understanding optimization in deep learning with central flows. *arXiv preprint arXiv:2410.24206*, 2024. 3
- Jacob Devlin. Bert: Pre-training of deep bidirectional transformers for language understanding. *arXiv preprint arXiv:1810.04805*, 2018. 2
- Alexey Dosovitskiy, Lucas Beyer, Alexander Kolesnikov, Dirk Weissenborn, Xiaohua Zhai, Thomas Unterthiner, Mostafa Dehghani, Matthias Minderer, Georg Heigold, Sylvain Gelly, et al. An image is worth 16x16 words: Transformers for image recognition at scale. *arXiv preprint arXiv:2010.11929*, 2020. 1
- Katie Everett, Lechao Xiao, Mitchell Wortsman, Alexander A Alemi, Roman Novak, Peter J Liu, Izzeddin Gur, Jascha Sohl-Dickstein, Leslie Pack Kaelbling, Jaehoon Lee, et al. Scaling exponents across parameterizations and optimizers. *arXiv preprint arXiv:2407.05872*, 2024. 3
- Leo Gao, Stella Biderman, Sid Black, Laurence Golding, Travis Hoppe, Charles Foster, Jason Phang, Horace He, Anish Thite, Noa Nabeshima, et al. The Pile: An 800GB dataset of diverse text for language modeling. *arXiv preprint arXiv:2101.00027*, 2020. 9, 16
- Thomas George, César Laurent, Xavier Bouthillier, Nicolas Ballas, and Pascal Vincent. Fast approximate natural gradient descent in a Kronecker-factored eigenbasis. *Advances in Neural Information Processing Systems*, 31, 2018. 5
- Aaron Gokaslan and Vanya Cohen. Openwebtext corpus. <http://SkyLion007.github.io/OpenWebTextCorpus>, 2019. 2, 9, 16
- Roger Grosse and James Martens. A Kronecker-factored approximate Fisher matrix for convolution layers. In *International Conference on Machine Learning*, pages 573–582. PMLR, 2016. 5
- Albert Gu and Tri Dao. Mamba: Linear-time sequence modeling with selective state spaces. *arXiv preprint arXiv:2312.00752*, 2023. 11
- Shengding Hu, Yuge Tu, Xu Han, Chaoqun He, Ganqu Cui, Xiang Long, Zhi Zheng, Yewei Fang, Yuxiang Huang, Weilin Zhao, et al. Minicpm: Unveiling the potential of small language models with scalable training strategies. *arXiv preprint arXiv:2404.06395*, 2024. 10
- Stanislaw Jastrzebski, Maciej Szymczak, Stanislav Fort, Devansh Arpit, Jacek Tabor, Kyunghyun Cho, and Krzysztof Geras. The break-even point on optimization trajectories of deep neural networks. In *International Conference on Learning Representations*, 2020. 3
- John Jumper, Richard Evans, Alexander Pritzel, Tim Green, Michael Figurnov, Olaf Ronneberger, Kathryn Tunyasuvunakool, Russ Bates, Augustin Žídek, Anna Potapenko, et al. Highly accurate protein structure prediction with alphafold. *nature*, 596(7873):583–589, 2021. 1
- Jean Kaddour. The MiniPile challenge for data-efficient language models. *arXiv preprint arXiv:2304.08442*, 2023. 2, 9, 16
- Andrej Karpathy. NanoGPT. <https://github.com/karpathy/nanoGPT>, 2022. 4, 16
- Jordan Keller et al. Muon optimizer. <https://github.com/KellerJordan/Muon?tab=readme-ov-file>, 2024. 3, 11

- Diederik P Kingma and Jimmy Ba. Adam: A method for stochastic optimization. *arXiv preprint arXiv:1412.6980*, 2014. [2](#)
- Frederik Kunstner, Robin Yadav, Alan Milligan, Mark Schmidt, and Alberto Bietti. Heavy-tailed class imbalance and why adam outperforms gradient descent on language models. *arXiv preprint arXiv:2402.19449*, 2024. [2](#), [6](#)
- Jimmy Lei Ba, Jamie Ryan Kiros, and Geoffrey E Hinton. Layer normalization. *ArXiv e-prints*, pages arXiv-1607, 2016. [4](#)
- Aixin Liu, Bei Feng, Bing Xue, Bingxuan Wang, Bochao Wu, Chengda Lu, Chenggang Zhao, Chengqi Deng, Chenyu Zhang, Chong Ruan, et al. Deepseek-v3 technical report. *arXiv preprint arXiv:2412.19437*, 2024a. [1](#)
- Hong Liu, Zhiyuan Li, David Hall, Percy Liang, and Tengyu Ma. Sophia: A scalable stochastic second-order optimizer for language model pre-training. *International Conference on Learning Representations*, 2024b. [3](#), [5](#), [17](#)
- Yinhan Liu, Myle Ott, Naman Goyal, Jingfei Du, Mandar Joshi, Danqi Chen, Omer Levy, Mike Lewis, Luke Zettlemoyer, and Veselin Stoyanov. Roberta: A robustly optimized bert pretraining approach. *arXiv preprint arXiv:1907.11692*, 2019. [9](#), [16](#)
- Ilya Loshchilov and Frank Hutter. Decoupled weight decay regularization. *arXiv preprint arXiv:1711.05101*, 2017. [2](#), [3](#)
- James Martens and Roger Grosse. Optimizing neural networks with Kronecker-factored approximate curvature. In *International conference on machine learning*, pages 2408–2417. PMLR, 2015. [4](#)
- Peng Mi, Li Shen, Tianhe Ren, Yiyi Zhou, Xiaoshuai Sun, Rongrong Ji, and Dacheng Tao. Make sharpness-aware minimization stronger: A sparsified perturbation approach. *Advances in Neural Information Processing Systems*, 35:30950–30962, 2022. [5](#)
- Weronika Ormaniec, Felix Dangel, and Sidak Pal Singh. What does it mean to be a transformer? insights from a theoretical hessian analysis. *arXiv preprint arXiv:2410.10986*, 2024. [3](#), [6](#), [7](#)
- Scott Pesme and Nicolas Flammarion. Saddle-to-saddle dynamics in diagonal linear networks. *Advances in Neural Information Processing Systems*, 2023. [2](#)
- Martin Popel and Ondřej Bojar. Training tips for the transformer model. *arXiv preprint arXiv:1804.00247*, 2018. [2](#)
- Alec Radford, Jeffrey Wu, Rewon Child, David Luan, Dario Amodei, and Ilya Sutskever. Language models are unsupervised multitask learners. *OpenAI blog*, 1(8):9, 2019. [2](#), [5](#), [16](#)
- Kwang Yong Shin, Suhyun Kim, and Soo-Mook Moon. Initializing the layer-wise learning rate, 2024. URL <https://openreview.net/forum?id=mSSiOzYkEA>. [3](#)
- Mohammad Shoeybi, Mostofa Patwary, Raul Puri, Patrick LeGresley, Jared Casper, and Bryan Catanzaro. Megatron-lm: Training multi-billion parameter language models using model parallelism. *arXiv preprint arXiv:1909.08053*, 2019. [8](#)
- Minhak Song, Kwangjun Ahn, and Chulhee Yun. Does sgd really happen in tiny subspaces? *arXiv preprint arXiv:2405.16002*, 2024. [3](#), [8](#)
- Jianlin Su, Murtadha Ahmed, Yu Lu, Shengfeng Pan, Wen Bo, and Yunfeng Liu. Roformer: Enhanced transformer with rotary position embedding. *Neurocomputing*, 568:127063, 2024. [16](#)
- Gemini Team, Rohan Anil, Sebastian Borgeaud, Jean-Baptiste Alayrac, Jiahui Yu, Radu Soricut, Johan Schalkwyk, Andrew M Dai, Anja Hauth, Katie Millican, et al. Gemini: a family of highly capable multimodal models. *arXiv preprint arXiv:2312.11805*, 2023. [1](#)
- Hugo Touvron, Thibaut Lavril, Gautier Izacard, Xavier Martinet, Marie-Anne Lachaux, Timothée Lacroix, Baptiste Rozière, Naman Goyal, Eric Hambro, Faisal Azhar, et al. Llama: Open and efficient foundation language models. *arXiv preprint arXiv:2302.13971*, 2023. [2](#), [5](#), [9](#), [16](#)

- Ashish Vaswani, Noam Shazeer, Niki Parmar, Jakob Uszkoreit, Llion Jones, Aidan N Gomez, Łukasz Kaiser, and Illia Polosukhin. Attention is all you need. *Advances in neural information processing systems*, 30, 2017. 1
- Nikhil Vyas, Depen Morwani, Rosie Zhao, Itai Shapira, David Brandfonbrener, Lucas Janson, and Sham Kakade. Soap: Improving and stabilizing shampoo using adam. *arXiv preprint arXiv:2409.11321*, 2024. 3
- Mingze Wang, Jinbo Wang, Haotian He, Zilin Wang, Guanhua Huang, Feiyu Xiong, Zhiyu Li, Lei Wu, et al. Improving generalization and convergence by enhancing implicit regularization. *Advances in Neural Information Processing Systems*, 2024a. 3, 5, 8, 17
- Mingze Wang et al. Understanding the expressive power and mechanisms of transformer for sequence modeling. *Advances in Neural Information Processing Systems*, 2024b. 1
- Kaiyue Wen, Zhiyuan Li, Jason Wang, David Hall, Percy Liang, and Tengyu Ma. Understanding warmup-stable-decay learning rates: A river valley loss landscape perspective. *arXiv preprint arXiv:2410.05192*, 2024. 3, 8, 10
- Thomas Wolf, Lysandre Debut, Victor Sanh, Julien Chaumond, Clement Delangue, Anthony Moi, Pierric Cistac, Tim Rault, Rémi Louf, Morgan Funtowicz, Joe Davison, Sam Shleifer, Patrick von Platen, Clara Ma, Yacine Jernite, Julien Plu, Canwen Xu, Teven Le Scao, Sylvain Gugger, Mariama Drame, Quentin Lhoest, and Alexander M. Rush. Transformers: State-of-the-art natural language processing. In *Proceedings of the 2020 Conference on Empirical Methods in Natural Language Processing: System Demonstrations*, pages 38–45, Online, October 2020. Association for Computational Linguistics. URL <https://www.aclweb.org/anthology/2020.emnlp-demos>. 6. 16
- Lei Wu, Chao Ma, and Weinan E. How SGD selects the global minima in over-parameterized learning: A dynamical stability perspective. *Advances in Neural Information Processing Systems*, 31:8279–8288, 2018. 3
- Xingyu Xie, Pan Zhou, Huan Li, Zhouchen Lin, and Shuicheng Yan. Adan: Adaptive nesterov momentum algorithm for faster optimizing deep models. *arXiv preprint arXiv:2208.06677*, 2022. 3
- Ruibin Xiong, Yunchang Yang, Di He, Kai Zheng, Shuxin Zheng, Chen Xing, Huishuai Zhang, Yanyan Lan, Liwei Wang, and Tiejun Liu. On layer normalization in the transformer architecture. In *International Conference on Machine Learning*, pages 10524–10533. PMLR, 2020. 2, 23
- Greg Yang, Edward J Hu, Igor Babuschkin, Szymon Sidor, Xiaodong Liu, David Farhi, Nick Ryder, Jakub Pachocki, Weizhu Chen, and Jianfeng Gao. Tensor programs v: Tuning large neural networks via zero-shot hyperparameter transfer. *arXiv preprint arXiv:2203.03466*, 2022. 3
- Zhilin Yang. Xlnet: Generalized autoregressive pretraining for language understanding. *arXiv preprint arXiv:1906.08237*, 2019. 3
- Huizhuo Yuan, Yifeng Liu, Shuang Wu, Xun Zhou, and Quanquan Gu. Mars: Unleashing the power of variance reduction for training large models. *arXiv preprint arXiv:2411.10438*, 2024. 3
- Biao Zhang and Rico Sennrich. Root mean square layer normalization. *Advances in Neural Information Processing Systems*, 32, 2019. 4
- Jingzhao Zhang, Sai Praneeth Karimireddy, Andreas Veit, Seungyeon Kim, Sashank Reddi, Sanjiv Kumar, and Suvrit Sra. Why are adaptive methods good for attention models? *Advances in Neural Information Processing Systems*, 33:15383–15393, 2020. 2
- Peiyuan Zhang, Guangtao Zeng, Tianduo Wang, and Wei Lu. Tinyllama: An open-source small language model, 2024a. 16
- Yushun Zhang, Congliang Chen, Tian Ding, Ziniu Li, Ruoyu Sun, and Zhi-Quan Luo. Why transformers need adam: A hessian perspective. *arXiv preprint arXiv:2402.16788*, 2024b. 2, 3, 6

Yushun Zhang, Congliang Chen, Ziniu Li, Tian Ding, Chenwei Wu, Yinyu Ye, Zhi-Quan Luo, and Ruoyu Sun. Adam-mini: Use fewer learning rates to gain more. *arXiv preprint arXiv:2406.16793*, 2024c. [1](#), [2](#), [3](#), [10](#), [19](#)

Jiawei Zhao, Zhenyu Zhang, Beidi Chen, Zhangyang Wang, Anima Anandkumar, and Yuandong Tian. Galore: Memory-efficient llm training by gradient low-rank projection. *arXiv preprint arXiv:2403.03507*, 2024. [3](#)

Appendix

| | |
|--|-----------|
| A Experimental Details | 16 |
| A.1 Training Configurations for AdamW Baselines | 16 |
| A.2 Experimental Details for Blockwise LR on AdamW | 17 |
| A.3 Experimental details for Adam-mini | 19 |
| B Proofs in Section 4 | 19 |
| B.1 Proof of Theorem 4.1 | 19 |
| B.2 Proof of Theorem 4.2 | 20 |
| B.3 Proof of Theorem 4.3 | 22 |

A Experimental Details

Models. We utilize two popular classes of LLM models for our pre-training experiments:

- **GPT-2.** We use GPT-2 (small) model (Radford et al., 2019), implemented via the nanoGPT code base (Karpathy, 2022). Following nanoGPT, the model employs Gaussian Error Linear Unit (GELU) activations and standard Layer Normalization (LayerNorm). Detailed model configurations are provided in Table 2.
- **LLaMA.** LLaMA (Touvron et al., 2023) is another popular decoder-only Transformer architecture, incorporating Rotary Positional Encoding (RoPE) (Su et al., 2024), Swish-Gated Linear Unit (SwiGLU), and Root mean square layer normalization (RMSNorm). We pre-train LLaMA models of sizes ranging from 0.13B to 1.1B parameters. For implementation, for 0.13B, 0.25B, 0.5B, 0.75B models, we utilize the LLaMA code from HuggingFace Transformers Library (Wolf et al., 2020). For the 1.1B model configuration, we follow TinyLlama (Zhang et al., 2024a), which employs grouped-query attention (Ainslie et al., 2023). Additional model configurations are detailed in Table 2.

Datasets. Models are pre-trained on the following datasets:

- **OpenWebText** (Gokaslan and Cohen, 2019). It is an opensource recreation of the WebText corpus, is extensively utilized for LLM pre-training such as RoBERTa (Liu et al., 2019) and GPT-2.
- **MiniPile.** (Kaddour, 2023). It is a 6GB subset of the deduplicated Pile (825GB) (Gao et al., 2020) presents a highly diverse text corpus. Given its diversity, training on minipile poses challenges and potential instabilities.

All experiments are conducted on 4 A800/H800 80G GPUs.

A.1 Training Configurations for AdamW Baselines

As a baseline optimizer, we use the default AdamW for LLM pre-training, configured with the hyperparameters $\beta_1 = 0.9, \beta_2 = 0.95$ and weight decay $\lambda = 0.1$. To ensure training stability, gradient clipping is applied by norm with threshold 1.0. These settings align with the training protocols used in nanoGPT and LLaMA models (Touvron et al., 2023). The LR strategy integrates a linear warm-up phase, followed by a cosine decay scheduler with the peak learning rate `lr_max` and the final learning rate `lr_min=lr_max/20`. Additionally,

Table 2: Model configurations and optimally-tuned peak learning rates.

| Acronym | Size | d_{model} | d_{FF} | n_head | depth | lr_max on OpenWebText | lr_max on MiniPile |
|---------------|-------|--------------------|-----------------|--------|-------|-----------------------|--------------------|
| GPT-2 (small) | 124M | 768 | 3072 | 12 | 12 | 6e-4 | 6e-4 |
| LLaMA (0.13B) | 134M | 768 | 3072 | 12 | 6 | – | 1.2e-3 |
| LLaMA (0.25B) | 237M | 1024 | 4096 | 16 | 8 | 8e-4 | 7.5e-4 |
| LLaMA (0.5B) | 522M | 1280 | 5120 | 20 | 15 | 8e-4 | 4.5e-4 |
| LLaMA (0.75B) | 743M | 1664 | 6656 | 26 | 13 | 6e-4 | – |
| LLaMA (1.1B) | 1175M | 2048 | 5632 | 32 | 22 | 4e-4 | – |

- **OpenWebText pre-training.** The (max) sequence length is set to 1024, and the batch size is set to 480, following nanoGPT and Liu et al. (2024b). The total training duration is 50,000 or 100,000 steps, including 1,000 warm-up steps. The grid search for lr_max is performed over {2e-4, 4e-4, 6e-4, 8e-4, 1e-3}. Optimal learning rates for each model are detailed in Table 2.
- **MiniPile pre-training.** The (max) sequence length is set to 512, and the batch size is set to 300, following Wang et al. (2024a). The total training duration is 30,000 or 60,000 steps, including 600 warm-up steps. The grid search for lr_max is performed over {3e-4, 4.5e-4, 6e-4, 7.5e-4, 9e-4, 1.2e-3, 1.5e-3}. Optimal learning rates for each model are detailed in Table 2.

Baselines: models are pre-trained using AdamW with the respective tuned lr_max for each dataset and model configuration.

Related Experiments.

- **Blockwise LR Experiments.** The baseline results in Figure 4, Figure 1 (right), and Table 1 (the w/o line) are trained following the configurations above.
- **Sharpness Principle Experiments.** Models for Figure 1 (left), Figure 2, Figure 3, are trained using the baseline configurations for GPT-2 (small) or LLaMA (0.25B) on OpenWebText, with a total training duration 50,000 steps. In these experiments, the sharpness is estimated using $h(\theta)$ in Eq. (3), with B set to 1024. The sharpness distributions and average sharpness values for different blocks (\bullet) are calculated on a logarithmic scale, i.e., $\log h(\theta[\bullet])$. Additionally, the experiment in Figure 7 employs the same model and sharpness estimator.
- **Theoretical Analysis Support.** To support our theoretical insights in Section 4.2, Figure 6 shows the evaluation of the parameter norms across different blocks during training. The model used is LLaMa (0.25B), trained on OpenWebText. The model is LLaMA (0.25B), trained on OpenWebText following the baseline configurations.

A.2 Experimental Details for Blockwise LR on AdamW

Switching Time. The principle of blockwise sharpness heterogeneity emerges clearly after the initial training phase, as shown in Figure 3. To leverage this principle, in our experiments of AdamW using Blockwise LR, we **switch** from standard AdamW to AdamW with Blockwise LR **at the end of LR warmup phase**.

Experiments in Figure 4. We adopt the adjusting ratios (5) as the default adjusting ratios for all experiments of AdamW with Blockwise LR.

Experiment on Hyper-parameter Tuning. We **only** tune the four adjusting ratios $r(\bullet)$ ($\bullet \in \{\text{Emb}, \text{QK}, \text{VO}, \text{FFN}\}$) in a single small-scale experiment: pre-training LLaMA (0.25B) on Minipile. Specifically, we compare the results under the following configurations of ratios:

$$\begin{aligned} r(\text{Emb}) &= 6, r(\text{QK}) = 4, r(\text{FFN}) = 3, r(\text{VO}) = 2; \\ r(\text{Emb}) &= 8, r(\text{QK}) = 6, r(\text{FFN}) = 4, r(\text{VO}) = 3; \\ r(\text{Emb}) &= 10, r(\text{QK}) = 8, r(\text{FFN}) = 6, r(\text{VO}) = 4. \end{aligned}$$

The results for the tuning experiments are presented in Figure 8. One can see that the configuration $r(\text{Emb}) = 10, r(\text{QK}) = 8, r(\text{FFN}) = 6, r(\text{VO}) = 4$ (Eq. (5)) achieves the largest improvement

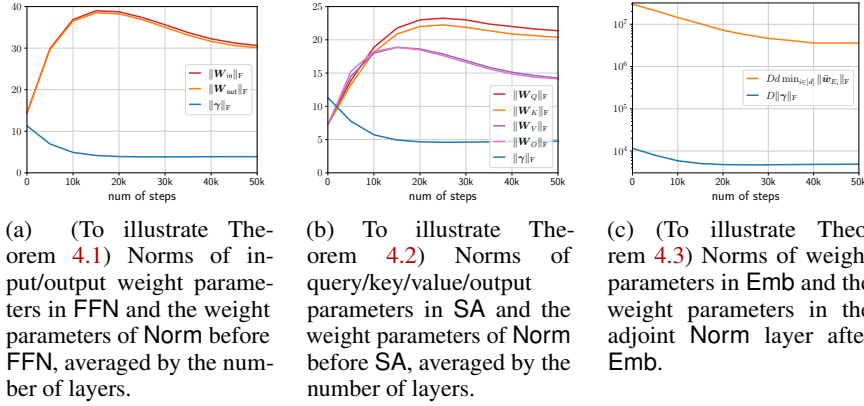


Figure 6: Evolution of parameter norms across different blocks during pre-training LLaMA (0.25B) on OpenWebText.

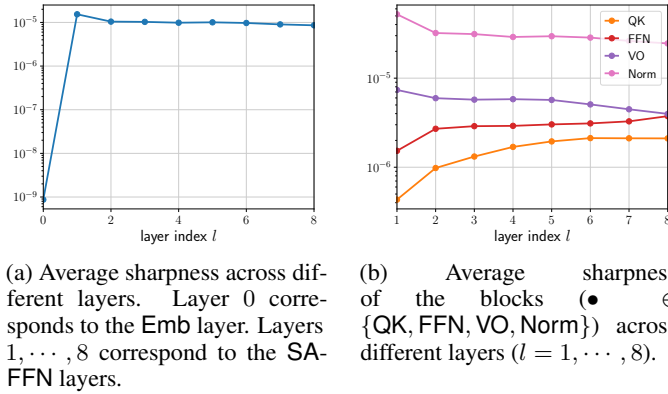


Figure 7: In a pre-trained LLaMA (0.25B) (with $L = 8$ layer), there is no clear disparity for the average sharpness across the **layers**. This is in stark contrast to our sharpness disparity **Principle (1)** across the **blocks**.

in terminal loss. Additionally, Blockwise LR demonstrates robustness to these ratios, consistently accelerating pre-training across all tested configurations.

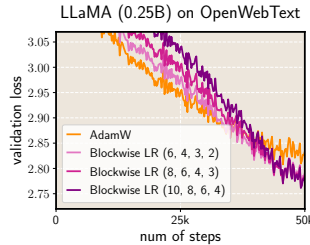


Figure 8: Pre-training LLaMA (0.25B) on Minipile using AdamW with Blockwise LR across three configurations of adjusting ratios.

Experiments in Table 1. We pre-train LLaMA (0.25B) on OpenWebText with a focusing on the three comparisons: (i) applying Blockwise LR exclusively to Emb; (ii) applying Blockwise LR to both Emb and FFN; (iii) applying Blockwise LR to blocks of all the four types (Emb, FFN, QK, and VO). The adjusting ratios are maintained as per the tuned in Eq. (5).

A.3 Experimental details for Adam-mini

Adam-mini Baseline. In the baseline experiments in Figure 5, following Zhang et al. (2024c), we adopt the same peak learning rate `lr_max` tuned for AdamW as the `lr_max` of Adam-mini.

Hyperparameter tuning. Since Adam-mini uses SGD within each blocks, its dynamics **differs significantly** from those of AdamW. Thus, for Adam-mini with Blockwise LR, we re-tune the ratios $r(\bullet) \in \{1, 2, 4\}$ for $\bullet \in \{\text{Emb}, \text{QK}, \text{FFN}, \text{VO}\}$. The tuned ratios are $r(\text{Emb}) = 4$, $r(\text{QK}) = 1$, $r(\text{FFN}) = 4$, $r(\text{VO}) = 4$, which are used in the experiments in Figure 5. Note that these ratios do not satisfy $r(\bullet) \propto \frac{S(\text{Norm})}{S(\bullet)}$. This discrepancy may stem from the unique dynamics of Adam-mini, particularly its SGD-like behavior within blocks. We leave further investigation for future work.

B Proofs in Section 4

B.1 Proof of Theorem 4.1

We focus on the transformation from $\mathbf{X}^{(l-1)}$ to $\mathbf{X}^{(l-1/2)}$:

$$\mathbf{X}^{(l)} = \mathbf{X}^{(l-1/2)} + \text{FFN}^{(l)} \left(\text{Norm}^l \left(\mathbf{X}^{(l-1/2)}; \gamma^{(l)} \right); \mathbf{W}_1^{(l)}, \mathbf{W}_2^{(l)} \right).$$

From the chain rule, it follows that:

$$\begin{aligned} \frac{\partial \mathcal{Q}}{\partial \mathbf{W}_\bullet^{(l)}} &= \frac{\partial \mathcal{Q}}{\partial \mathbf{X}^{(l)}} \frac{\partial \mathbf{X}^{(l)}}{\partial \mathbf{W}_\bullet^{(l)}}, \quad \bullet \in \{1, 2\}; \\ \frac{\partial \mathcal{Q}}{\partial \gamma^{(l)}} &= \frac{\partial \mathcal{Q}}{\partial \mathbf{X}^{(l)}} \frac{\partial \mathbf{X}^{(l)}}{\partial \gamma^{(l)}}. \end{aligned}$$

Thus, it suffices to compute $\frac{\partial \mathbf{X}^{(l)}}{\partial \mathbf{W}_\bullet^{(l)}}$ and $\frac{\partial \mathbf{X}^{(l)}}{\partial \gamma^{(l)}}$. For simplicity, we define:

$$\begin{aligned} \mathbf{X} &:= \mathbf{X}^{(l-1/2)}, \quad \mathbf{X}_{\text{std}} = \frac{\mathbf{X} - \mathbb{E}_r[\mathbf{X}]}{\sqrt{\mathbb{V}_r[\mathbf{X}]}}, \quad \mathbf{X}_{\text{Norm}} := \text{Norm}(\mathbf{X}; \gamma) = \mathbf{X}_{\text{std}} \odot (\mathbf{1}_{n \times 1} \otimes \gamma), \\ \mathbf{M} &:= \mathbf{X}_{\text{Norm}} \mathbf{W}_1, \quad \mathbf{A} := \sigma(\mathbf{M}), \quad \mathbf{F} := \mathbf{A} \mathbf{W}_2, \quad \mathbf{Y} := \mathbf{X}^{(l)} = \mathbf{X} + \mathbf{F}, \end{aligned}$$

where $\sigma(\cdot)$ represents the ReLU or Leaky ReLU activation function. We now compute $\frac{\partial \mathbf{Y}}{\partial \mathbf{W}_\bullet}$ and $\frac{\partial \mathbf{Y}}{\partial \gamma}$.

It is straightforward that:

$$\begin{aligned} \frac{\partial \mathbf{Y}}{\partial \mathbf{W}_1} &= \frac{\partial \mathbf{F}}{\partial \mathbf{W}_1} = \frac{\partial \mathbf{F}}{\partial \mathbf{A}} \frac{\partial \mathbf{A}}{\partial \mathbf{M}} \frac{\partial \mathbf{M}}{\partial \mathbf{W}_1} = (\mathbf{I}_n \otimes \mathbf{W}_2^\top) \frac{\partial \mathbf{A}}{\partial \mathbf{M}} (\mathbf{X}_{\text{Norm}} \otimes \mathbf{I}_M); \\ \frac{\partial \mathbf{Y}}{\partial \gamma} &= \frac{\partial \mathbf{F}}{\partial \mathbf{X}_{\text{Norm}}} \frac{\partial \mathbf{X}_{\text{Norm}}}{\partial \gamma} = \frac{\partial \mathbf{F}}{\partial \mathbf{A}} \frac{\partial \mathbf{A}}{\partial \mathbf{M}} \frac{\partial \mathbf{M}}{\partial \mathbf{X}_{\text{Norm}}} \frac{\partial \mathbf{X}_{\text{Norm}}}{\partial \gamma} \\ &= (\mathbf{I}_n \otimes \mathbf{W}_2^\top) \frac{\partial \mathbf{A}}{\partial \mathbf{M}} (\mathbf{I}_n \otimes \mathbf{W}_1^\top) \left(\text{diag}(\text{vec}(\mathbf{X}_{\text{std}})) (\mathbf{1}_{n \times 1} \otimes \mathbf{I}_D) \right). \end{aligned}$$

For the (Leaky) ReLU, it holds that $\sigma(z) = z\sigma'(z)$. Thus, for $\frac{\partial \mathbf{Y}}{\partial \mathbf{W}_2}$, we have:

$$\frac{\partial \mathbf{Y}}{\partial \mathbf{W}_2} = \frac{\partial \mathbf{F}}{\partial \mathbf{W}_2} = \mathbf{A} \otimes \mathbf{I}_D = \left(\mathbf{X}_{\text{Norm}} \mathbf{W}_1 \odot \frac{\partial \mathbf{A}}{\partial \mathbf{M}} \right) \otimes \mathbf{I}_D.$$

Now we derive the upper bounds. First, notice that:

$$\|\mathbf{X}_{\text{std}}\|_F = \left(\sum_{i=1}^n \left(\frac{\mathbf{X}_{i,:} - \mathbb{E}[\mathbf{X}_{i,:}]}{\sqrt{\mathbb{V}[\mathbf{X}_{i,:}]}} \right)^2 \right)^{1/2} = \left(\sum_{i=1}^n D \right)^{1/2} = \sqrt{nD};$$

$$\|\mathbf{X}_{\text{Norm}}\|_{\text{F}} = \|\mathbf{X}_{\text{std}} \odot (\mathbf{1}_{n \times 1} \otimes \gamma)\|_{\text{F}} \leq \|\mathbf{X}_{\text{std}}\|_{\text{F}} \|\mathbf{1}_{n \times 1} \otimes \gamma\|_{\text{F}} \leq \sqrt{nD} \|\mathbf{1}_{n \times 1}\|_{\text{F}} \|\gamma\|_{\text{F}} \leq n\sqrt{D} \|\gamma\|_{\text{F}}.$$

Consequently, we have the following estimates:

$$\begin{aligned} & \left\| \frac{\partial \mathcal{Q}}{\partial \mathbf{W}_1} \right\|_{\text{F}} \leq \left\| \frac{\partial \mathcal{Q}}{\partial \mathbf{Y}} \right\|_{\text{F}} \left\| \frac{\partial \mathbf{Y}}{\partial \mathbf{W}_1} \right\|_{\text{F}} = \left\| \frac{\partial \mathcal{Q}}{\partial \mathbf{Y}} \right\|_{\text{F}} \left\| (\mathbf{I}_n \otimes \mathbf{W}_2^\top) \frac{\partial \mathbf{A}}{\partial \mathbf{M}} (\mathbf{X}_{\text{Norm}} \otimes \mathbf{I}_M) \right\|_{\text{F}} \\ & \leq \left\| \frac{\partial \mathcal{Q}}{\partial \mathbf{Y}} \right\|_{\text{F}} \left\| \frac{\partial \mathbf{A}}{\partial \mathbf{M}} \right\|_{\text{F}} \|\mathbf{I}_n \otimes \mathbf{W}_2^\top\|_2 \|\mathbf{X}_{\text{Norm}} \otimes \mathbf{I}_M\|_2 \leq \left\| \frac{\partial \mathcal{Q}}{\partial \mathbf{Y}} \right\|_{\text{F}} \left\| \frac{\partial \mathbf{A}}{\partial \mathbf{M}} \right\|_{\text{F}} \|\mathbf{I}_n\|_2 \|\mathbf{I}_M\|_2 \|\mathbf{W}_2^\top\|_{\text{F}} \|\mathbf{X}_{\text{Norm}}\|_{\text{F}} \\ & \leq \left\| \frac{\partial \mathcal{Q}}{\partial \mathbf{Y}} \right\|_{\text{F}} \left\| \frac{\partial \mathbf{A}}{\partial \mathbf{M}} \right\|_{\text{F}} \|\mathbf{W}_2\|_{\text{F}} \|\mathbf{X}_{\text{Norm}}\|_{\text{F}} \leq n\sqrt{D} \left\| \frac{\partial \mathcal{Q}}{\partial \mathbf{Y}} \right\|_{\text{F}} \left\| \frac{\partial \mathbf{A}}{\partial \mathbf{M}} \right\|_{\text{F}} \|\mathbf{W}_2\|_{\text{F}} \|\gamma\|_{\text{F}}; \end{aligned}$$

$$\begin{aligned} & \left\| \frac{\partial \mathcal{Q}}{\partial \mathbf{W}_2} \right\|_{\text{F}} \leq \left\| \frac{\partial \mathcal{Q}}{\partial \mathbf{Y}} \right\|_{\text{F}} \left\| \frac{\partial \mathbf{Y}}{\partial \mathbf{W}_2} \right\|_{\text{F}} = \left\| \frac{\partial \mathcal{Q}}{\partial \mathbf{Y}} \right\|_{\text{F}} \left\| \left(\mathbf{X}_{\text{Norm}} \mathbf{W}_1 \odot \frac{\partial \mathbf{A}}{\partial \mathbf{M}} \right) \otimes \mathbf{I}_D \right\|_{\text{F}} \\ & \leq \left\| \frac{\partial \mathcal{Q}}{\partial \mathbf{Y}} \right\|_{\text{F}} \left\| \left(\mathbf{X}_{\text{Norm}} \mathbf{W}_1 \odot \frac{\partial \mathbf{A}}{\partial \mathbf{M}} \right) \right\|_{\text{F}} \|\mathbf{I}_D\|_2 \leq \left\| \frac{\partial \mathcal{Q}}{\partial \mathbf{Y}} \right\|_{\text{F}} \left\| \frac{\partial \mathbf{A}}{\partial \mathbf{M}} \right\|_{\text{F}} \|\mathbf{X}_{\text{Norm}} \mathbf{W}_1\|_{\text{F}} \\ & \leq \left\| \frac{\partial \mathcal{Q}}{\partial \mathbf{Y}} \right\|_{\text{F}} \left\| \frac{\partial \mathbf{A}}{\partial \mathbf{M}} \right\|_{\text{F}} \|\mathbf{W}_1\|_{\text{F}} \|\mathbf{X}_{\text{Norm}}\|_{\text{F}} \leq n\sqrt{D} \left\| \frac{\partial \mathcal{Q}}{\partial \mathbf{Y}} \right\|_{\text{F}} \left\| \frac{\partial \mathbf{A}}{\partial \mathbf{M}} \right\|_{\text{F}} \|\mathbf{W}_1\|_{\text{F}} \|\gamma\|_{\text{F}}; \end{aligned}$$

$$\begin{aligned} & \left\| \frac{\partial \mathcal{Q}}{\partial \gamma} \right\|_{\text{F}} \leq \left\| \frac{\partial \mathcal{Q}}{\partial \mathbf{Y}} \right\|_{\text{F}} \left\| \frac{\partial \mathbf{Y}}{\partial \gamma} \right\|_{\text{F}} \\ & = \left\| \frac{\partial \mathcal{Q}}{\partial \mathbf{Y}} \right\|_{\text{F}} \left\| (\mathbf{I}_n \otimes \mathbf{W}_2^\top) \frac{\partial \mathbf{A}}{\partial \mathbf{M}} (\mathbf{I}_n \otimes \mathbf{W}_1^\top) \left(\text{diag}(\text{vec}(\mathbf{X}_{\text{std}})) (\mathbf{1}_{n \times 1} \otimes \mathbf{I}_D) \right) \right\|_{\text{F}} \\ & \leq \left\| \frac{\partial \mathcal{Q}}{\partial \mathbf{Y}} \right\|_{\text{F}} \left\| \frac{\partial \mathbf{A}}{\partial \mathbf{M}} \right\|_{\text{F}} \|\mathbf{I}_n \otimes \mathbf{W}_2^\top\|_{\text{F}} \|\mathbf{I}_n \otimes \mathbf{W}_1^\top\|_{\text{F}} \|\text{diag}(\text{vec}(\mathbf{X}_{\text{std}})) (\mathbf{1}_{n \times 1} \otimes \mathbf{I}_D)\|_{\text{F}} \\ & \leq \left\| \frac{\partial \mathcal{Q}}{\partial \mathbf{Y}} \right\|_{\text{F}} \left\| \frac{\partial \mathbf{A}}{\partial \mathbf{M}} \right\|_{\text{F}} \|\mathbf{I}_n\|_2 \|\mathbf{W}_2\|_{\text{F}} \|\mathbf{I}_n\|_2 \|\mathbf{W}_1\|_{\text{F}} \|\text{diag}(\text{vec}(\mathbf{X}_{\text{std}}))\|_{\text{F}} \|\mathbf{1}_{n \times 1} \otimes \mathbf{I}_D\|_{\text{F}} \\ & \leq \left\| \frac{\partial \mathcal{Q}}{\partial \mathbf{Y}} \right\|_{\text{F}} \left\| \frac{\partial \mathbf{A}}{\partial \mathbf{M}} \right\|_{\text{F}} \|\mathbf{W}_1\|_{\text{F}} \|\mathbf{W}_2\|_{\text{F}} \|\mathbf{X}_{\text{std}}\|_{\text{F}} \|\mathbf{1}_{n \times 1}\|_{\text{F}} \|\mathbf{I}_D\|_2 \\ & \leq n\sqrt{D} \left\| \frac{\partial \mathcal{Q}}{\partial \mathbf{Y}} \right\|_{\text{F}} \left\| \frac{\partial \mathbf{A}}{\partial \mathbf{M}} \right\|_{\text{F}} \|\mathbf{W}_1\|_{\text{F}} \|\mathbf{W}_2\|_{\text{F}}. \end{aligned}$$

Thus, if we define

$$\Psi := n\sqrt{D} \left\| \frac{\partial \mathcal{Q}}{\partial \mathbf{Y}} \right\|_{\text{F}} \left\| \frac{\partial \mathbf{A}}{\partial \mathbf{M}} \right\|_{\text{F}} \|\mathbf{W}_1\|_{\text{F}} \|\mathbf{W}_2\|_{\text{F}} \|\gamma\|_{\text{F}},$$

then it holds that:

$$\left\| \frac{\partial \mathcal{Q}}{\partial \mathbf{W}_1} \right\|_{\text{F}} \leq \frac{\Psi}{\|\mathbf{W}_1\|_{\text{F}}}; \quad \left\| \frac{\partial \mathcal{Q}}{\partial \mathbf{W}_2} \right\|_{\text{F}} \leq \frac{\Psi}{\|\mathbf{W}_2\|_{\text{F}}}; \quad \left\| \frac{\partial \mathcal{Q}}{\partial \gamma} \right\|_{\text{F}} \leq \frac{\Psi}{\|\gamma\|_{\text{F}}}$$

Therefore,

$$\begin{aligned} \mathcal{S}(\mathbf{W}_\bullet) &= \frac{1}{\#(\mathbf{W}_\bullet)} \left\| \frac{\partial \mathcal{Q}}{\partial \mathbf{W}_\bullet} \right\|_{\text{F}}^2 = \mathcal{O} \left(\frac{\Psi^2}{D^2 \|\mathbf{W}_\bullet\|_{\text{F}}^2} \right), \quad \bullet \in \{1, 2\}; \\ \mathcal{S}(\gamma) &= \frac{1}{\#(\gamma)} \left\| \frac{\partial \mathcal{Q}}{\partial \gamma} \right\|_{\text{F}}^2 = \mathcal{O} \left(\frac{\Psi^2}{D \|\gamma\|_{\text{F}}^2} \right). \end{aligned}$$

B.2 Proof of Theorem 4.2

We focus on the transformation from $\mathbf{X}^{(l-1)}$ to $\mathbf{X}^{(l-1/2)}$:

$$\mathbf{X}^{(l-1/2)} = \mathbf{X}^{(l-1)} + \text{SA}^{(l)} \left(\text{Norm}^{(l-1/2)} \left(\mathbf{X}^{(l-1)}; \gamma^{(l-1/2)} \right); \mathbf{W}_K^{(l)}, \mathbf{W}_Q^{(l)}, \mathbf{W}_V^{(l)}, \mathbf{W}_O^{(l)} \right).$$

From the chain rule, it follows that:

$$\begin{aligned}\frac{\partial Q}{\partial \mathbf{W}_\bullet^{(l)}} &= \frac{\partial Q}{\partial \mathbf{X}^{(l-1/2)}} \frac{\partial \mathbf{X}^{(l-1/2)}}{\partial \mathbf{W}_\bullet^{(l)}}, \quad \bullet \in \{K, Q, V, O\}; \\ \frac{\partial Q}{\partial \gamma^{(l-1/2)}} &= \frac{\partial Q}{\partial \mathbf{X}^{(l-1/2)}} \frac{\partial \mathbf{X}^{(l-1/2)}}{\partial \gamma^{(l-1/2)}}.\end{aligned}$$

Thus, it suffices to compute $\frac{\partial \mathbf{X}^{(l-1/2)}}{\partial \mathbf{W}_\bullet^{(l-1/2)}}$ and $\frac{\partial \mathbf{X}^{(l-1/2)}}{\partial \gamma^{(l-1/2)}}$. For simplicity, we define:

$$\begin{aligned}\mathbf{X} &:= \mathbf{X}^{(l-1)}, \quad \mathbf{X}_{\text{std}} = \frac{\mathbf{X} - \mathbb{E}_r[\mathbf{X}]}{\sqrt{\mathbb{V}_r[\mathbf{X}]}, \quad \mathbf{X}_{\text{Norm}} := \text{Norm}(\mathbf{X}; \gamma) = \mathbf{X}_{\text{std}} \odot \gamma, \\ \mathbf{M} &:= \frac{\mathbf{X}_{\text{Norm}} \mathbf{W}_Q \mathbf{W}_K^\top \mathbf{X}_{\text{Norm}}^\top}{\sqrt{D}}, \quad \mathbf{A} := \text{softmax}(\mathbf{M}), \quad \mathbf{S} := \mathbf{A} \mathbf{X}_{\text{Norm}} \mathbf{W}_V \mathbf{W}_O, \\ \mathbf{Y} &:= \mathbf{X}^{(l-1/2)} = \mathbf{X} + \mathbf{S}.\end{aligned}$$

We now compute $\frac{\partial \mathbf{Y}}{\partial \mathbf{W}_\bullet}$ and $\frac{\partial \mathbf{Y}}{\partial \gamma}$:

$$\begin{aligned}\frac{\partial \mathbf{Y}}{\partial \mathbf{W}_Q} &= \frac{\partial \mathbf{S}}{\partial \mathbf{W}_Q} = \frac{\partial \mathbf{S}}{\partial \mathbf{A}} \frac{\partial \mathbf{A}}{\partial \mathbf{M}} \frac{\partial \mathbf{M}}{\partial \mathbf{W}_Q} = (\mathbf{I}_n \otimes \mathbf{W}_O^\top \mathbf{W}_V^\top \mathbf{X}_{\text{Norm}}^\top) \frac{\partial \mathbf{A}}{\partial \mathbf{M}} \left(\frac{\mathbf{X}_{\text{Norm}} \otimes \mathbf{X}_{\text{Norm}} \mathbf{W}_K}{\sqrt{D}} \right); \\ \frac{\partial \mathbf{Y}}{\partial \mathbf{W}_K} &= \frac{\partial \mathbf{S}}{\partial \mathbf{W}_K} = \frac{\partial \mathbf{S}}{\partial \mathbf{A}} \frac{\partial \mathbf{A}}{\partial \mathbf{M}} \frac{\partial \mathbf{M}}{\partial \mathbf{W}_K} = (\mathbf{I}_n \otimes \mathbf{W}_O^\top \mathbf{W}_V^\top \mathbf{X}_{\text{Norm}}^\top) \frac{\partial \mathbf{A}}{\partial \mathbf{M}} \left(\frac{\mathbf{X}_{\text{Norm}} \otimes \mathbf{X}_{\text{Norm}} \mathbf{W}_Q}{\sqrt{D}} \right); \\ \frac{\partial \mathbf{Y}}{\partial \mathbf{W}_V} &= \frac{\partial \mathbf{S}}{\partial \mathbf{W}_V} = \mathbf{A} \mathbf{X}_{\text{Norm}} \otimes \mathbf{W}_O^\top; \\ \frac{\partial \mathbf{Y}}{\partial \mathbf{W}_O} &= \frac{\partial \mathbf{S}}{\partial \mathbf{W}_O} = \mathbf{A} \mathbf{X}_{\text{Norm}} \mathbf{W}_V \otimes \mathbf{I}_D.\end{aligned}$$

Moreover,

$$\begin{aligned}\frac{\partial \mathbf{Y}}{\partial \gamma} &= \frac{\partial \mathbf{Y}}{\partial \mathbf{X}_{\text{Norm}}} \frac{\partial \mathbf{X}_{\text{Norm}}}{\partial \gamma} = \frac{\partial \mathbf{S}}{\partial \mathbf{X}_{\text{Norm}}} \frac{\partial \mathbf{X}_{\text{Norm}}}{\partial \gamma} \\ &= \left(\frac{1}{\sqrt{D}} (\mathbf{I}_n \otimes \mathbf{W}_O^\top \mathbf{W}_V^\top \mathbf{X}_{\text{Norm}}^\top) \frac{\partial \mathbf{A}}{\partial \mathbf{M}} \left((\mathbf{I}_n \otimes \mathbf{X}_{\text{Norm}} \mathbf{W}_K \mathbf{W}_Q^\top) + \mathbf{K}_{n,n} (\mathbf{I}_n \otimes \mathbf{X}_{\text{Norm}} \mathbf{W}_Q \mathbf{W}_K^\top) \right) \right. \\ &\quad \left. + \mathbf{A} \otimes \mathbf{W}_O^\top \mathbf{W}_V^\top \right) \left(\text{diag}(\text{vec}(\mathbf{X}_{\text{std}})) (\mathbf{1}_{n \times 1} \otimes \mathbf{I}_d) \right),\end{aligned}$$

where $\mathbf{K}_{n,n}$ is the commutation matrix³.

Recalling the proof in Appendix B.1, we have:

$$\|\mathbf{X}_{\text{std}}\|_F = \sqrt{nD}, \quad \|\mathbf{X}_{\text{Norm}}\|_F \leq n\sqrt{D} \|\gamma\|_F.$$

Then, similar to the proof in Appendix B.1, we have the following upper bounds:

$$\begin{aligned}\left\| \frac{\partial Q}{\partial \mathbf{W}_Q} \right\|_F &\leq \frac{1}{\sqrt{D}} \left\| \frac{\partial Q}{\partial \mathbf{Y}} \right\|_F \left\| \frac{\partial \mathbf{A}}{\partial \mathbf{M}} \right\|_F \|\mathbf{W}_K\|_F \|\mathbf{W}_V\|_F \|\mathbf{W}_O\|_F \|\mathbf{X}_{\text{Norm}}\|_F^3 \\ &\leq \frac{(n\sqrt{D})^3}{\sqrt{D}} \left\| \frac{\partial Q}{\partial \mathbf{Y}} \right\|_F \left\| \frac{\partial \mathbf{A}}{\partial \mathbf{M}} \right\|_F \|\mathbf{W}_K\|_F \|\mathbf{W}_V\|_F \|\mathbf{W}_O\|_F \|\gamma\|_F^3; \\ \left\| \frac{\partial Q}{\partial \mathbf{W}_K} \right\|_F &\leq \frac{1}{\sqrt{D}} \left\| \frac{\partial Q}{\partial \mathbf{Y}} \right\|_F \left\| \frac{\partial \mathbf{A}}{\partial \mathbf{M}} \right\|_F \|\mathbf{W}_Q\|_F \|\mathbf{W}_V\|_F \|\mathbf{W}_O\|_F \|\mathbf{X}_{\text{Norm}}\|_F^3\end{aligned}$$

³The commutation matrix $\mathbf{K}_{m,n}$ transforms column-wise vectorization into row-wise vectorization.

$$\begin{aligned}
&\leq \frac{(n\sqrt{D})^3}{\sqrt{D}} \left\| \frac{\partial Q}{\partial \mathbf{Y}} \right\|_{\mathbb{F}} \left\| \frac{\partial \mathbf{A}}{\partial \mathbf{M}} \right\|_{\mathbb{F}} \|\mathbf{W}_K\|_{\mathbb{F}} \|\mathbf{W}_Q\|_{\mathbb{F}} \|\mathbf{W}_V\|_{\mathbb{F}} \|\mathbf{W}_O\|_{\mathbb{F}} \|\gamma\|_{\mathbb{F}}^3; \\
\left\| \frac{\partial Q}{\partial \mathbf{W}_V} \right\|_{\mathbb{F}} &\leq \left\| \frac{\partial Q}{\partial \mathbf{Y}} \right\|_{\mathbb{F}} \|\mathbf{A}\|_{\mathbb{F}} \|\mathbf{W}_O\|_{\mathbb{F}} \|\mathbf{X}_{\text{Norm}}\|_{\mathbb{F}} \leq n\sqrt{D} \left\| \frac{\partial Q}{\partial \mathbf{Y}} \right\|_{\mathbb{F}} \|\mathbf{A}\|_{\mathbb{F}} \|\mathbf{W}_O\|_{\mathbb{F}} \|\gamma\|_{\mathbb{F}}; \\
\left\| \frac{\partial Q}{\partial \mathbf{W}_O} \right\|_{\mathbb{F}} &\leq \left\| \frac{\partial Q}{\partial \mathbf{Y}} \right\|_{\mathbb{F}} \|\mathbf{A}\|_{\mathbb{F}} \|\mathbf{W}_V\|_{\mathbb{F}} \|\mathbf{X}_{\text{Norm}}\|_{\mathbb{F}} \leq n\sqrt{D} \left\| \frac{\partial Q}{\partial \mathbf{Y}} \right\|_{\mathbb{F}} \|\mathbf{A}\|_{\mathbb{F}} \|\mathbf{W}_V\|_{\mathbb{F}} \|\gamma\|_{\mathbb{F}}; \\
\left\| \frac{\partial Q}{\partial \gamma} \right\|_{\mathbb{F}} &\leq \left\| \frac{\partial Q}{\partial \mathbf{Y}} \right\|_{\mathbb{F}} \sqrt{n} \|\mathbf{X}_{\text{std}}\|_{\mathbb{F}} \left(\frac{2}{\sqrt{D}} \left\| \left(\mathbf{I}_n \otimes \mathbf{W}_O^{\top} \mathbf{W}_V^{\top} \mathbf{X}_{\text{Norm}}^{\top} \right) \frac{\partial \mathbf{A}}{\partial \mathbf{M}} \left(\mathbf{I}_n \otimes \mathbf{X}_{\text{Norm}} \mathbf{W}_K \mathbf{W}_Q^{\top} \right) \right\|_{\mathbb{F}} + \|\mathbf{A} \otimes \mathbf{W}_O^{\top} \mathbf{W}_V^{\top}\|_{\mathbb{F}} \right) \\
&\leq n\sqrt{D} \left\| \frac{\partial Q}{\partial \mathbf{Y}} \right\|_{\mathbb{F}} \left(\frac{2}{\sqrt{D}} \left\| \frac{\partial \mathbf{A}}{\partial \mathbf{M}} \right\|_{\mathbb{F}} \|\mathbf{W}_K\|_{\mathbb{F}} \|\mathbf{W}_Q\|_{\mathbb{F}} \|\mathbf{W}_V\|_{\mathbb{F}} \|\mathbf{W}_O\|_{\mathbb{F}} \|\mathbf{X}_{\text{Norm}}\|_{\mathbb{F}}^2 + \|\mathbf{A}\|_{\mathbb{F}} \|\mathbf{W}_V\|_{\mathbb{F}} \|\mathbf{W}_O\|_{\mathbb{F}} \right) \\
&\leq \left\| \frac{\partial Q}{\partial \mathbf{Y}} \right\|_{\mathbb{F}} \left(\frac{2(n\sqrt{D})^3}{\sqrt{D}} \left\| \frac{\partial \mathbf{A}}{\partial \mathbf{M}} \right\|_{\mathbb{F}} \|\mathbf{W}_K\|_{\mathbb{F}} \|\mathbf{W}_Q\|_{\mathbb{F}} \|\mathbf{W}_V\|_{\mathbb{F}} \|\mathbf{W}_O\|_{\mathbb{F}} \|\gamma\|_{\mathbb{F}}^2 + n\sqrt{D} \|\mathbf{A}\|_{\mathbb{F}} \|\mathbf{W}_V\|_{\mathbb{F}} \|\mathbf{W}_O\|_{\mathbb{F}} \right).
\end{aligned}$$

Therefore, if we define:

$$\begin{aligned}
\Phi &:= \frac{(n\sqrt{D})^3}{\sqrt{D}} \left\| \frac{\partial Q}{\partial \mathbf{Y}} \right\|_{\mathbb{F}} \left\| \frac{\partial \mathbf{A}}{\partial \mathbf{M}} \right\|_{\mathbb{F}} \|\mathbf{W}_K\|_{\mathbb{F}} \|\mathbf{W}_Q\|_{\mathbb{F}} \|\mathbf{W}_V\|_{\mathbb{F}} \|\mathbf{W}_O\|_{\mathbb{F}} \|\gamma\|_{\mathbb{F}}^3, \\
\Psi &:= n\sqrt{D} \left\| \frac{\partial Q}{\partial \mathbf{Y}} \right\|_{\mathbb{F}} \|\mathbf{A}\|_{\mathbb{F}} \|\mathbf{W}_V\|_{\mathbb{F}} \|\mathbf{W}_O\|_{\mathbb{F}} \|\gamma\|_{\mathbb{F}},
\end{aligned}$$

then it holds that:

$$\begin{aligned}
\left\| \frac{\partial Q}{\partial \mathbf{W}_K} \right\|_{\mathbb{F}} &\leq \frac{\Phi}{\|\mathbf{W}_K\|_{\mathbb{F}}}; & \left\| \frac{\partial Q}{\partial \mathbf{W}_Q} \right\|_{\mathbb{F}} &\leq \frac{\Phi}{\|\mathbf{W}_Q\|_{\mathbb{F}}}; \\
\left\| \frac{\partial Q}{\partial \mathbf{W}_V} \right\|_{\mathbb{F}} &\leq \frac{\Psi}{\|\mathbf{W}_V\|_{\mathbb{F}}}; & \left\| \frac{\partial Q}{\partial \mathbf{W}_O} \right\|_{\mathbb{F}} &\leq \frac{\Psi}{\|\mathbf{W}_O\|_{\mathbb{F}}}; \\
\left\| \frac{\partial Q}{\partial \gamma} \right\|_{\mathbb{F}} &\leq \frac{2\Phi + \Psi}{\|\gamma\|_{\mathbb{F}}}.
\end{aligned}$$

Therefore,

$$\begin{aligned}
\mathcal{S}(\mathbf{W}_{\bullet}) &= \frac{1}{\#(\mathbf{W}_{\bullet})} \left\| \frac{\partial Q}{\partial \mathbf{W}_{\bullet}} \right\|_{\mathbb{F}}^2 = \mathcal{O} \left(\frac{\Phi^2}{D^2 \|\mathbf{W}_{\bullet}\|_{\mathbb{F}}^2} \right), \quad \bullet \in \{K, Q\}; \\
\mathcal{S}(\mathbf{W}_{\bullet}) &= \frac{1}{\#(\mathbf{W}_{\bullet})} \left\| \frac{\partial Q}{\partial \mathbf{W}_{\bullet}} \right\|_{\mathbb{F}}^2 = \mathcal{O} \left(\frac{\Psi^2}{D^2 \|\mathbf{W}_{\bullet}\|_{\mathbb{F}}^2} \right), \quad \bullet \in \{V, O\}; \\
\mathcal{S}(\gamma) &= \frac{1}{\#(\gamma)} \left\| \frac{\partial Q}{\partial \gamma} \right\|_{\mathbb{F}}^2 = \mathcal{O} \left(\frac{\Phi^2 + \Psi^2}{D \|\gamma\|_{\mathbb{F}}^2} \right).
\end{aligned}$$

B.3 Proof of Theorem 4.3

We focus on the transformation from \mathbf{X} to $\mathbf{Y} := \text{Norm}(\mathbf{X} \mathbf{W}_E; \gamma^{(1/2)})$. For simplicity, we define:

$$\mathbf{Z} := \mathbf{X} \mathbf{W}_E, \quad \mathbf{Z}_{\text{std}} := \frac{\mathbf{Z} - \mathbb{E}_r[\mathbf{Z}]}{\sqrt{\mathbb{Z}_r[\mathbf{Z}]}} \quad \mathbf{Y} = \text{Norm}(\mathbf{Z}; \gamma) = \mathbf{Z}_{\text{std}} \odot (\mathbf{1}_{n \times 1} \otimes \gamma).$$

It is straightforward that:

$$\frac{\partial \mathbf{Y}}{\partial \gamma} = \text{diag}(\text{vec}(\mathbf{Z}_{\text{std}})) (\mathbf{1}_{n \times 1} \otimes \mathbf{I}_D).$$

Recalling the proof in Appendix B.1, we have:

$$\left\| \frac{\partial \mathbf{Y}}{\partial \boldsymbol{\gamma}} \right\|_{\text{F}} \leq n\sqrt{D}.$$

Then we calculate $\frac{\partial \mathbf{Y}}{\partial \tilde{\mathbf{W}}_E}$. For simplicity, we denote

$$\begin{aligned} \tilde{\mathbf{Z}} &:= \mathbf{Z} - \mathbb{E}_r[\mathbf{Z}], \quad \mathbf{Z} = \begin{pmatrix} \tilde{z}_1 \\ \dots \\ \tilde{z}_d \end{pmatrix} \in \mathbb{R}^{d \times D}, \\ \tilde{\mathbf{W}}_E &:= \mathbf{W}_E - \mathbb{E}_r[\mathbf{W}_E], \quad \mathbf{W}_E = \begin{pmatrix} \mathbf{w}_{E_1} \\ \dots \\ \mathbf{w}_{E_d} \end{pmatrix} \in \mathbb{R}^{d \times D}, \quad \tilde{\mathbf{W}}_E = \begin{pmatrix} \tilde{\mathbf{w}}_{E_1} \\ \dots \\ \tilde{\mathbf{w}}_{E_d} \end{pmatrix} \in \mathbb{R}^{d \times D} \end{aligned}$$

By the proof in Xiong et al. (2020), for a vector $\mathbf{x} \in \mathbb{R}^{1 \times D}$, denoted by $\tilde{\mathbf{x}} := \mathbf{x} - \mathbb{E}[\mathbf{x}]$, then $\frac{\partial \mathbf{x}_{\text{std}}}{\partial \mathbf{x}} = \frac{\sqrt{D}}{\|\tilde{\mathbf{x}}\|_2} \left(\mathbf{I} - \frac{\tilde{\mathbf{x}} \tilde{\mathbf{x}}^\top}{\|\tilde{\mathbf{x}}\|_2^2} \right) \left(\mathbf{I} - \frac{1}{d} \mathbf{1}_{1 \times D} \mathbf{1}_{1 \times D}^\top \right)$. Thus, we have:

$$\begin{aligned} \frac{\partial \mathbf{Y}}{\partial \tilde{\mathbf{W}}_E} &= \frac{\partial \mathbf{Y}}{\partial \mathbf{Z}_{\text{std}}} \frac{\partial \mathbf{Z}_{\text{std}}}{\partial \mathbf{Z}} \frac{\partial \mathbf{Z}}{\partial \tilde{\mathbf{W}}_E} \\ &= (\mathbf{I}_n \otimes \text{diag}(\text{vec}(\boldsymbol{\gamma}))) \text{diag} \left(\left\{ \frac{\sqrt{D}}{\|\tilde{\mathbf{z}}_i\|_2} \left(\mathbf{I} - \frac{\tilde{\mathbf{z}}_i \tilde{\mathbf{z}}_i^\top}{\|\tilde{\mathbf{z}}_i\|_2^2} \right) \left(\mathbf{I} - \frac{1}{D} \mathbf{1}_{1 \times D} \mathbf{1}_{1 \times D}^\top \right) \right\}_{i \in [n]} \right) (\mathbf{X} \otimes \mathbf{I}_D). \end{aligned}$$

Recalling the relationship $z_{i,j} = \sum_{k=1}^d x_{i,k} w_{k,j}$, we have $\mathbb{E}[z_i] = \sum_{k=1}^d x_{i,k} \mathbb{E}[w_k]$, which implies

$$\tilde{\mathbf{z}}_i = \sum_{k=1}^d x_{i,k} \tilde{\mathbf{w}}_k.$$

Combining this property with the that are one-hot fact of the inputs \mathbf{X} , we have:

$$\min_{i \in [n]} \|\tilde{\mathbf{z}}_i\|_2 \geq \min_{k \in [d]} \|\tilde{\mathbf{w}}_k\|_2.$$

Additionally, the one-hot encoding ensures:

$$\|\mathbf{X}\|_{\text{F}} = \left(\sum_{i=1}^n x_{i,j}^2 \right)^{1/2} = \sqrt{n}.$$

Now we have the following bound:

$$\begin{aligned} &\left\| \frac{\partial \mathbf{Y}}{\partial \tilde{\mathbf{W}}_E} \right\|_{\text{F}} \\ &\leq \|\mathbf{I}_n \otimes \text{diag}(\text{vec}(\boldsymbol{\gamma}))\|_{\text{F}} \left\| \text{diag} \left(\left\{ \frac{\sqrt{D}}{\|\tilde{\mathbf{z}}_i\|_2} \left(\mathbf{I} - \frac{\tilde{\mathbf{z}}_i \tilde{\mathbf{z}}_i^\top}{\|\tilde{\mathbf{z}}_i\|_2^2} \right) \left(\mathbf{I} - \frac{1}{D} \mathbf{1}_{1 \times D} \mathbf{1}_{1 \times D}^\top \right) \right\}_{i \in [n]} \right) \right\|_2 \|\mathbf{X} \otimes \mathbf{I}_D\|_2 \\ &\leq \sqrt{n} \|\boldsymbol{\gamma}\|_{\text{F}} \frac{\sqrt{D}}{\min_{i \in [n]} \|\tilde{\mathbf{z}}_i\|_2} \|\mathbf{X}\|_2 \leq n\sqrt{D} \frac{\|\boldsymbol{\gamma}\|_{\text{F}}}{\min_{i \in [n]} \|\tilde{\mathbf{z}}_i\|_2} \leq n\sqrt{D} \frac{\|\boldsymbol{\gamma}\|_{\text{F}}}{\min_{i \in [d]} \|\tilde{\mathbf{w}}_i\|_2}. \end{aligned}$$

If we choose $\Psi := n\sqrt{D} \|\boldsymbol{\gamma}\|_{\text{F}}$, then we have:

$$\left\| \frac{\partial \mathbf{Y}}{\partial \boldsymbol{\gamma}} \right\|_{\text{F}} \leq \frac{\Psi}{\|\boldsymbol{\gamma}\|_{\text{F}}}, \quad \left\| \frac{\partial \mathbf{Y}}{\partial \tilde{\mathbf{W}}_E} \right\|_{\text{F}} \leq \frac{\Psi}{\min_{i \in [d]} \|\tilde{\mathbf{w}}_i\|_2}.$$

Therefore,

$$\begin{aligned} \mathcal{S}(\mathbf{W}_E) &= \frac{1}{\#(\mathbf{W}_E)} \left\| \frac{\partial \mathcal{Q}}{\partial \tilde{\mathbf{W}}_E} \right\|_{\text{F}}^2 = \mathcal{O} \left(\frac{\Psi^2}{Dd \min_{i \in [d]} \|\tilde{\mathbf{w}}_i\|_2^2} \right); \\ \mathcal{S}(\boldsymbol{\gamma}) &= \frac{1}{\#(\boldsymbol{\gamma})} \left\| \frac{\partial \mathcal{Q}}{\partial \boldsymbol{\gamma}} \right\|_{\text{F}}^2 = \mathcal{O} \left(\frac{\Psi^2}{D \|\boldsymbol{\gamma}\|_{\text{F}}^2} \right). \end{aligned}$$